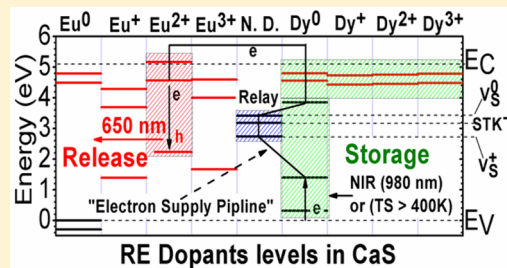


Native Point Defects in CaS: Focus on Intrinsic Defects and Rare Earth Ion Dopant Levels for Up-converted Persistent Luminescence

Bolong Huang*

Department of Physics and Materials Science, City University of Hong Kong, Kowloon, Hong Kong SAR, China

ABSTRACT: We studied native point defects as well as Eu and Dy ion doping in CaS by the simple DFT + Hubbard U method. The electronic properties and formation energies of native point defects and dopants have been discussed. We found the neutral S vacancy has the lowest energy of 0.62 eV under the Ca-rich limit. The Schottky pair is another dominant defect with a cost of 1.51 eV per defect site from S-rich to Ca-rich chemical potential limits. Our calculations on the thermodynamic transition levels confirm the experimental observed intrinsic blue two-peak broad band emissions stimulated by near-infrared range irradiation for undoped CaS. Both Eu and Dy show an energetic favorable trend to be substitutionally doped in the CaS lattice. All of the positive charge states of the Eu ion contribute localized recombination trapping level in the gap while having very deep donor transition levels. The neutral state of Dy contributes to the occupied 4f level localized 1.3 eV below the conduction band edge with very shallow donor type transition level (0^{+/−}) of 0.56 eV below the conduction band. All of the positive charge states of Dy have two shallow 5d levels with 0.4 and 0.6 eV below the conduction band. In this work, we further analyzed that the Dy dopant contributed deeper trap levels in the CaS materials that can store the electron carriers with more evenly, wider, and deeper range of levels distributed so that they lengthen the decay-time of the persistent luminescence. The related 980 nm photo-stimulated luminescence is actualized with the help of native defects like V_S⁰, V_S⁺, and STK[−] as relay centers for a possible up-converted luminescence. We also summarized a narrow doping limit energy which has been determined as 1.33 eV constantly in CaS independent to different chemical potential limits. This gives a solid theoretical reference for lanthanide ion doping experiments in CaS.



INTRODUCTION

Stronger intensity, longer time, and lower cost with flexible wavelength in persistent luminescence are increasingly needed as demands for biochemical and materials engineering rapidly expand. Persistent luminescence, which is based on the long-decay-time phosphorescence concept,^{1–3} are challenged to down-scale to smaller nanosized particle synthesis with lower cost and longer time for in vivo imaging. The rare-earth metal ions assisted phosphor luminescence technique has aroused tremendous interest in biological, chemical, and physical applications,^{4–10} which play a leading role on modulating luminescence properties.

It is necessary to understand the mechanism of persistent luminescence, which is closely related to the phosphor storage feature of some particular wide band gap materials like CaS. According to the left panel of Figure 1, the existence of intrinsic defects of the material can lead to a relatively “long-self-sustained” luminescence (from minutes to hours) in ambient conditions after excitations cease. This storage and release of energy in terms of the electron transfer mechanism¹¹ are assisted by the intrinsic defects, whose level is at about 1.5 eV below the conduction band acting as a reservoir to accommodate the excited electrons from valence bands. This energy separation is therefore easily covered by NIR ranged irradiation to thermally stimulate the accommodated electrons to jump back into the delocalized conduction band or through the quantum tunneling effect, followed by multiphonon nonradiative lattice relaxation to the metastable emission state. As we know, the localized holes

also stabilized at the intrinsic defect sites such as metal vacancies, whose levels are below the emission state. The delocalized electrons will recombine such holes and release the photons in terms of luminescence (radiative luminescence).

To modulate the emission wavelength, doping is a popular technology. Rare-earth (RE) metal ions as dopants have fine-structure levels of f-orbitals (4f for lanthanides and 5f actinides) to emit the specific wavelength light we need. As illustrated in the right panel of Figure 1, the RE dopant contributes 4f and 5d levels for electron–hole recombination, whose emission state is just below the conduction band. The second type of RE ion dopant has deeper trap levels than the intrinsic defect levels of host materials, which prolongs the duration of the luminescence and extends the electron relaxation time from deeper levels. As reviewed by Smet et al., the synthesis of CaS as a good phosphor can be found as early as 1700 by Friedrich Hoffmann.¹² However, even to date, there is still a lack of comprehensive understanding on the intrinsic electronic and optical properties of crystal CaS in relation to its native point defects. Similar materials like alkali halide (NaCl, LiF, etc.) or oxides (CaO, MgO,¹³ etc.) have a variety of color emissions by the F centers induced by anion vacancies. Such an F center contains the natively trapped electrons within the band gap, and their electronic trapping levels determine the optical emission properties. A recent theoretical

Received: September 9, 2015

Published: November 23, 2015

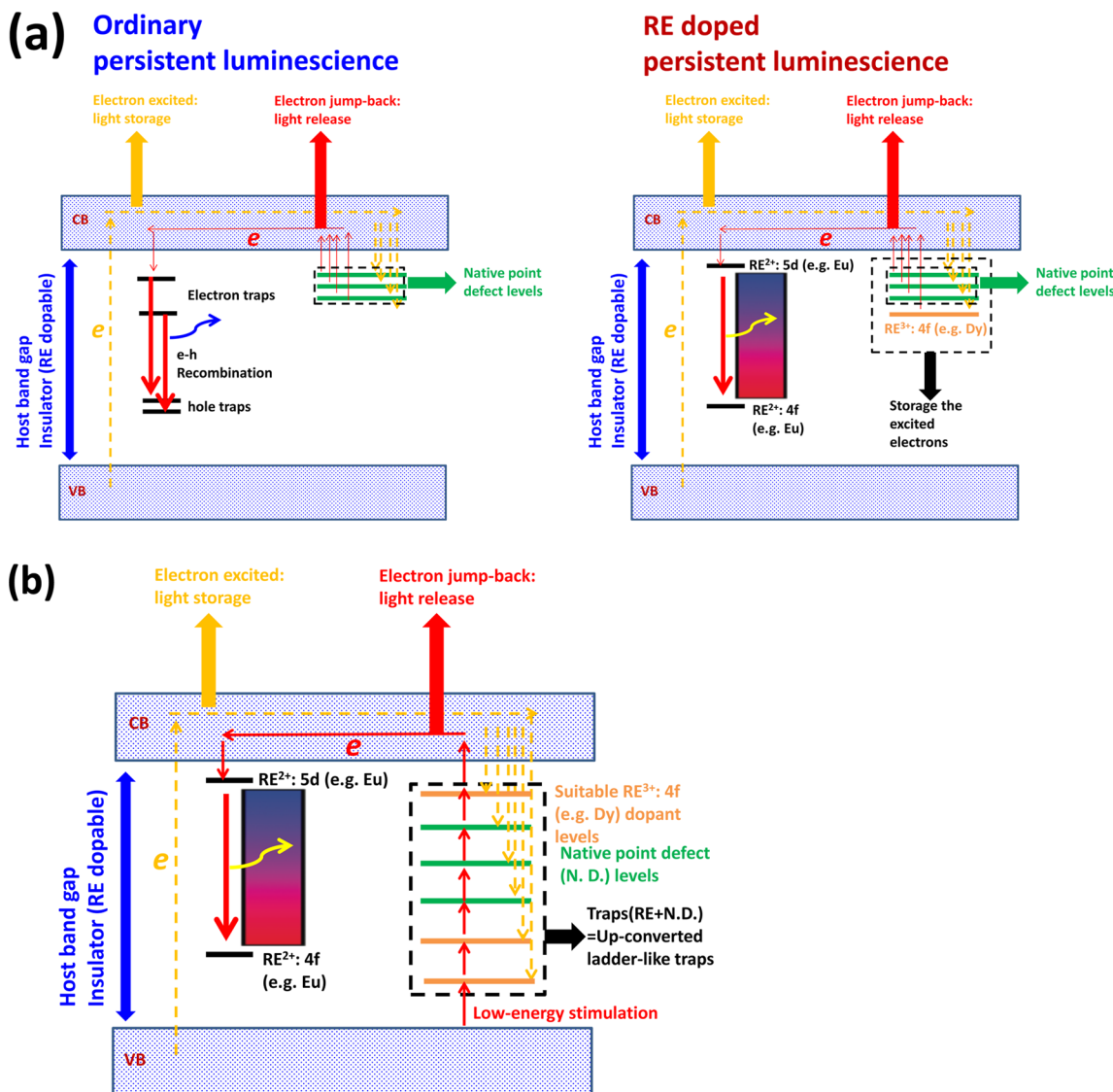


Figure 1. (a) Schematic processes of ordinary (undoped) and RE doped insulators for persistent luminescence (both light storage and release) related to the dopant levels and native point defect levels. (b) Schematic process of up-converted persistent luminescence with the combined energy trap levels from the native point defects and suitably chosen RE dopants.

study on calcium aluminate (CaAl_2O_4) shows that the native point defects and rare-earth dopant play a subtle role mutually in affecting its luminescence properties.^{14,15}

A recent persistent and photo-stimulated luminescence (PSL) experiment was conducted based on both CaS:Eu^{2+} and Dy^{3+} upon UV and 980 nm photoirradiations, respectively.^{7,16} Such persistent luminescence can be explained by the carriers (electrons/holes) at the shallow trap level conduction band minimum (CBM) stimulated into the conduction band by photo-irradiation and recombined at the acceptor levels given by cation dopants like Eu^{2+} . The Dy^{3+} is as deep as 1.3 eV below the CBM together with intrinsic defect levels for efficient activation by 980 nm irradiation toward persistent luminescence. X-ray powder diffraction (XRPD) results confirm the simple cubic symmetry ($Fm\bar{3}m$) for what the synthesized nanoparticle CaS:Eu^{2+} possesses.⁷ Therefore, such advanced optical materials applications also lead us to have a preliminary understanding of the native defect states of crystal CaS and confirmation on the charge transfer mechanism^{2,11} by ab initio calculations.

It has been a long debate to explain the mechanism of persistent luminescence by doping of rare-earth metal ions. The proposed “hole-transfer mechanism” by Matsuzawa et al.² explains the role of Eu ion in persistent luminescence in SrAl_2O_4 or similar insulators² with induction of unordinary valence state of Eu (e.g., Eu^+), while other experiments argued that there are no valence changes during whole process of stimulation and luminescence.^{17–19} They also attempted to know the stability of Eu^+ through ab initio calculation. Dorenbos¹¹ proposed a necessary electron transport mechanism based on experiments to demonstrate the stability of Eu^{3+} and Dy^{2+} . Thus, we aim to use the simplest material like CaS to understand the electronic localization levels as well as the effect of native point defect levels of host materials. To maintain persistent luminescence with specific wavelength, it is significant to confirm which charge state of Eu ion contributes to the localized levels in the band gap.

In the past few years, many advance first-principles methods like DFT, DFT+U, hybrid functionals,^{20–22} and GW methods have been well performed on many solids. However, for DFT+U, based on self-consistently determined Hubbard U on the cation’s

d-orbital and anion's p-orbital, the self-interaction error (SIE) can be reduced into an acceptably low level that recovers behaviors of both localized electrons and holes states. Note that to accurately describe the electron/hole interactions that bind the F-center trapping level in the solids, an appropriate magnitude of the hole localization on anion sites is required. This helps us to obtain accurate F-center excitation energies to meet the photoirradiation in persistent and PSL studies.^{7,12} Besides, it is also necessary to obtain detailed knowledge of the electronic structure of CaS, in particular the nature of the unoccupied density of states near the conduction band edge or minimum (CBM), as this causes much attention on the consideration of the 3d orbitals of Ca into valence electron wave functions during ab initio calculations. Whether the 3d orbitals of Ca are to be treated as fully empty or partially filled (e.g., $3d^\delta$ with $0 < \delta < 1$) is also a question to be carefully taken into account. This will be discussed in the following section.

EXPERIMENTAL SECTION

We chose the cubic lattice with the same symmetry of rocksalt (NaCl) for modeling the crystal CaS. The simple calculations of GGA+U with a rotational invariant scheme²³ was used from the CASTEP code.²⁴ The norm-conserving pseudopotentials of Ca and S are generated by the OPIUM code in the Kleinman-Bylander projector form²⁵ and the already employed nonlinear partial core correction²⁶ to reduce the atomic core-valence electron density overlap. We treated the (3s, 3p, 3d, and 4s) states as valence states of Ca. The RRKJ method is chosen as the optimization of pseudopotentials.²⁷ As we know, the norm-conserving pseudopotentials can reflect all-electron behavior for outer shell valence electrons with $|S\text{-matrix}| = 1$ compared to ultrasoft pseudopotentials.^{28,29} Since both Ca and S are relatively light elements, the spin-orbit coupling effect has not been considered in the calculations. The PBE functional was chosen for PBE+U calculations with a kinetic cutoff energy of 850 eV, which expands the valence electrons states in a plane-wave basis set. The ensemble DFT (EDFT) method of Marzari et al.³⁰ is used for reducing the charge-sloshing effect during the electronic minimization of solving the Kohn-Sham equation. Reciprocal space integration was performed by k -point grids of $10 \times 10 \times 10 k$ points in the Brillouin zone of CaS. This converges the total energy to under 5.0×10^{-7} eV per atom. The Hellmann-Feynman force on each atom was converged to lower than 0.01 eV/Å.

We follow the Anisimov type DFT+U method²³ and the self-consistently determined Hubbard U parameter for Ca 3d orbital by our new linear response method. To stabilize the hole states lying in the S 3p orbitals, we also apply a self-consistently determined Hubbard U potential (method used above) to the S 3p states following Lany,^{22,31} Morgan et al.,³² and Keating et al.³³ Accordingly, both the d- and p-orbital electrons of the cations and anions should be considered when using DFT+U.³⁴ For defects, we use a $2 \times 2 \times 2$ CaS supercell containing 64 atoms. We select the (1/4, 1/4, 1/4) special k -point³⁵ in the simple cubic $2 \times 2 \times 2$ supercell. The geometry optimization used the Broyden-Fletcher-Goldfarb-Shannon (BFGS) algorithm through all bulk and defect supercell calculations.

Another key setting is the pseudopotential for Ca. We generated the norm-conserving pseudopotential orbitals with $3s^2 3p^6 4s^2$ for Ca by the OPIUM code. The $3d^0$ configuration is also considered in the generation. This does not change the valence distribution but will increase the accuracy of the valence electron interaction of Ca. In real DFT calculations, the $3d^0$ and $4s^2$ of Ca will have a certain overlap with the occupancy of 0.4–0.5 e through Mulliken analysis. This caused us to consider an on-site Hubbard U energy reserved for this fractionally occupied empty 3d orbital for Ca. Such consideration of $3d^\delta$ ($0 < \delta < 1$) is also verified in the electronic structure calculations and experiments of CaB₆, which is a new semiconductor for spin electronics.^{36–38} In that, the structure has 3d of Ca hybridized with 2p orbitals of the anions affecting the band gap size of the Brillouin zone.³⁹ For the total plane wave basis set for Ca, we use the 850 eV that was suggested by Clark et al. with similar norm-conserving generations.⁴⁰ With our self-consistently

determined process,⁴¹ the on-site Hubbard U parameters for 3d of Ca and 2p of S are 2.51 and 5.14 eV, respectively.

For the RE ions used in the CaS calculations, we use the self-consistent determination for the U correction on the localized 4f orbitals to correct the on-site Coulomb energy of the electron spurious self-energy. The detailed process was in a previous work.⁴¹ The self-consistently determined U parameters for DFT+U calculations on the Eu and Dy ion doping in CaS was presented here as 7.80 and 6.31 eV. For the pseudopotentials of the Eu and Dy used for calculation, we similarly chose a nonlinear core correction technique for correcting the valence-core charge density overlapping in such heavy fermions elements. A detailed discussion of such a method has been presented in previous work about the native point defect study of CeO₂.³⁴ The valence electron configurations for the pseudopotentials we chose for the generation are $4f^6$ for Eu³⁺ as ground state configuration and are similar for the Dy³⁺ with $4f^9$ for the ground state as well. All of the DFT+U calculations have been performed on the norm-conserving pseudopotential theoretical scheme. This will help us to reflect the all-electron behavior of the valence electrons especially for the subtle effect of the 4f electrons and the outer 6s electrons.

For the calculation of defect formation energy in different charge states, the overall supercell size was kept fixed based on the relaxed neutral bulk unit cell. The defect formation energy (H_q) at the charge state q as a function of the Fermi energy (E_F) and the chemical potential $\Delta\mu$ of element α is given by

$$H_q(E_F, \mu) = [E_q - E_H] + q(E_V + \Delta E_F) + \sum_{\alpha} n_{\alpha}(\mu_{\alpha}^0 + \Delta\mu_{\alpha}) \quad (1)$$

where E_q and E_H are the total energy of a defect cell and a perfect cell, respectively, q is the calculated charge, ΔE_F is the Fermi energy with respect to the valence band maximum, n_{α} is the number of atoms of element α , and μ_{α}^0 is the reference chemical potential, following Lany and Zunger.⁴²

RESULTS AND DISCUSSION

Bulk CaS. CaS has a rock-salt structure with a symmetry of $Fm\bar{3}m$ with a lattice parameter of about 5.70 Å. The relaxed structure of ground state by DFT+U has a lattice parameter of 5.84 Å with a small error of +2%. From Figure 2, the electronic

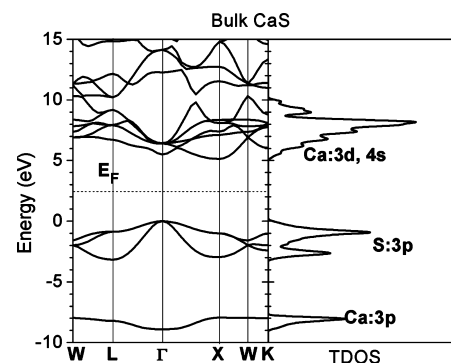


Figure 2. Band structure and TDOS of bulk CaS.

band structure calculations based on the optimized cell got a 5.13 eV indirect band gap from the Γ to X transition, close to the results reported by Capobianco et al.⁷ The direct transition gap of $\Gamma \rightarrow \Gamma$ is 5.55 eV is close to the result of 5.57 eV reported by Poncé et al. using the GW method.⁴³ Another direct transition gap of X → X is 6.14 eV, which is 1.0 eV higher than the results from Poncé et al.⁴³ The valence bandwidth we got is 3.25 eV, and the conduction bandwidth is 3.69 eV. The valence band (from -3.3 to 0 eV in Figure 2) is contributed by 3p orbitals of S, while the fulfilled 3p level of Ca is down to the -8 eV relative to

the highest occupied level (0 eV). The conduction band is mainly contributed by 3d and 4s orbitals of Ca, and the lowest unoccupied level is dominant by the 3d level of Ca. These are remarkably consistent with the results calculated by both Tran-Blaha 09 (TB09) and the many-body GW method from Waroquier et al.⁴⁴ Moreover, we see that with both applied Hubbard U parameters on the 3d of Ca and 3p of S, the electronic structure calculation substantially improves not only the band gap but also the nearly consistent valence and conduction band widths, respectively. This also can be seen from the previous work.³⁴

For the bulk formation enthalpy of crystal CaS, $\mu_{Ca} + \mu_S = \Delta H_f(CaS)$, and the experimental formation enthalpy of CaS is reported as -5.00 eV at $T = 298$ K (-482.4 kJ/mol).⁴⁵ Our calculations give -5.01 eV by GGA+U ($U_d = 2.51$, $U_p = 5.14$) at $T = 0$ K (ground state), which agrees well with the experimental value at $T = 298$ K.

S Vacancy (V_S). The V_S could be seen as an F center defect in CaS. V_S with charge states of 0, +1, and +2 has been investigated. The neutral V_S^0 left two electrons lying at nearby Ca sites with antiferromagnetic (AFM) behavior for the electronic states all over the Brillouin zone, as shown in Figure 3a. The two localized states showing spin-up and down with 1.72 eV lower than the CBM. These two states are indeed provided by the two electrons that had fallen into the overlapped 3d–4s orbitals of neighboring Ca, which were originally left by the S vacancy (V_S). Their energy levels are degenerated, hence giving s-like wave functions. These overlapped 3d–4s orbitals of Ca in fact form the trapping levels that carry the excess electrons at the defect sites. This is very different from the other ionic compounds like alkali halide (NaCl, LiF, etc.) which only consist of s–p orbitals.⁴⁶

The V_S^+ also gives two localized states within the band gap but with one empty; the orbitals of the states are also given by the 3d–4s orbitals. As there is only one electron at the V_S^+ site, these 3d–4s trapping levels split due to the different electron occupancies, as shown in Figure 3a. The filled trap level is 1.23 eV lower than the empty trap level, while the empty trap level is 1.16 eV lower than the CBM. Different from the total density of states (TDOS) of V_S^0 , the singly positive V_S^+ presents a ferromagnetic (FM) behavior due to the absence of energy degeneration of the 3d–4s trap levels for the localized electrons of V_S site. However, the empty state is actually the trap levels of the localized hole states in CaS with V_S , and the hole trap level is actually 1.23 eV higher than the electron trap level at the ground states and *vice versa* for the excitation states like 980 nm photoirradiation experimentally (this means that the electron level is 1.23 eV lower than the excited level). Gao et al. has studied the similar CaB₆, which is another Ca-based ionic compound; their more accurate electron energy loss spectroscopy (EELS) experiments suggested that the Ca with d orbitals actively acts as an ionic hole that transfers the charge from the s, p, and d states.³⁹ This gives evidence to prove our explanations of the split of the two trap levels.

The V_S^{2+} turns back to the AFM state with two aligned spin-up and down empty states within the band gap. Both of them also return to the degenerated energy levels for the 3d–4s trap level. Those empty trap levels are sitting 1.67 eV below the CBM. Another evident change for the electronic states of the V_S in CaS is the band edges from the TDOS in Figure 3a. The valence band edge is almost unchanged within those three different charge states (0, +1, and +2), while the conduction band edges have obvious variations near the CBM. Thus, we deduce that the localized electrons left by V_S are only interacting with the 3d and 4s orbitals of Ca and have no interactions and effects on the

3p orbitals of nearby S sites. These electrons trapped at the V_S sites are in fact from the neighboring Ca ions. In all, the lattice and electronic behaviors of V_S in CaS match the F center in ionic compounds, as shown in Figure 3b by schematic diagrams. Owing to the structural feature, the nearest neighbors of V_S are all at the Ca site. As can be seen from Figure 3c, the V_S^0 has no lattice distortion effects, but the V_S^+ makes an evident distortion that pushes the six Ca sites outward while attracting the nearest S sites little inward. The V_S^{2+} shows the distortion more vastly. The localized electron orbitals all have an s-like wave function feature, while the localized hole state shows some extent of hybridized d-orbitals.

From the angle of defect formation energies, Figure 3d shows that the V_S in CaS is a positive-effective correlation energy (+ U_{eff}) defect ($U_{eff} = +0.75$ eV), which has been discussed in the work of Zeng et al.¹⁵ This accordingly shows that the process of $2 V_S^+ \rightarrow V_S^0 + V_S^{2+}$ is an endothermal chemical reaction. It is known that forming each charge state of V_S follows different extents of local lattice distortions, while the total energy costs of these thermally ionized V_S defect states cannot be compensated for by the lattice distortions. Therefore, it comes with a positive U_{eff} and V_S^+ is also proved to be a widely existing defect in such host ionic crystals found by the electron spin resonance (ESR) measurements, which is generally called the F⁺ center. Under S-rich chemical potential limits, the V_S^0 cost 5.63 eV to form, while it has an as low as 0.62 eV formation energy under the Ca-rich limit. For the F⁺ center defect, V_S^+ has energies of 1.76 eV and -3.25 eV under S-rich and Ca-rich limits, respectively. The V_S transition levels of (+2/+1) and (+1/0) states are 3.12 and 3.87 eV, respectively, which are 2.01 and 1.26 eV below the CBM. By the aspect of formation energy, the (+1/0) state in fact matches the transition level requirement of the persistent luminescence predicted by Capobianco et al.⁷

S Interstitial (S_i). The S_i in CaS could be a strong acceptor center that gives the localized hole states trapping ability, but it could be a localized electron–hole trapping complex depending on the local bonding feature. For instance, the O interstitials (O_i) in metal oxides may form peroxides with O–O homopolar bonds in the lattice, whose π -electrons localized along the O–O bond at the O_i sites, as shown in previous work on metal oxides.³⁴ The neutral S_i in CaS with the S–S bond induces four localized levels with spin-degeneration as shown in Figure 4a. One of the localized electronic trap levels is at about 0.2 eV higher than the valence band maximum (VBM). The other two levels are -4.3 eV and -5.0 eV, below the VBM. They all have π -like electronic orbital features. The fourth localizes at 0.4 eV below the CBM presenting as a π^* orbital for the antibonding state of the S–S bond by S_i .

For the singly negative S_i in CaS (S_i^-), in the band gap shown in Figure 4a, there are four gap states for trapping the electrons and holes. Two lined up as spin-up and down with about 0.7 eV above the VBM, the second spin-up trap level for the localized electron locates 3.1 eV higher than the VBM, while being 1.39 eV below the second spin-down trap states for the localized hole.

The doubly negative S_i^{2-} in CaS has occupied deep levels with 1.53 eV above the VBM as shown in Figure 4a, which are spin-paired in terms of antiferromagnetic behavior at the same highest occupied level (0 eV). These states are mainly induced by the two excess electrons but experienced the repulsive Coulomb potential from electrons occupied in the host, where the original highest occupied level is the VBM in Figure 4a.

Figure 4b shows that the localized electron and hole orbitals are all along the S–S bond direction induced by relaxed S_i^- sites.

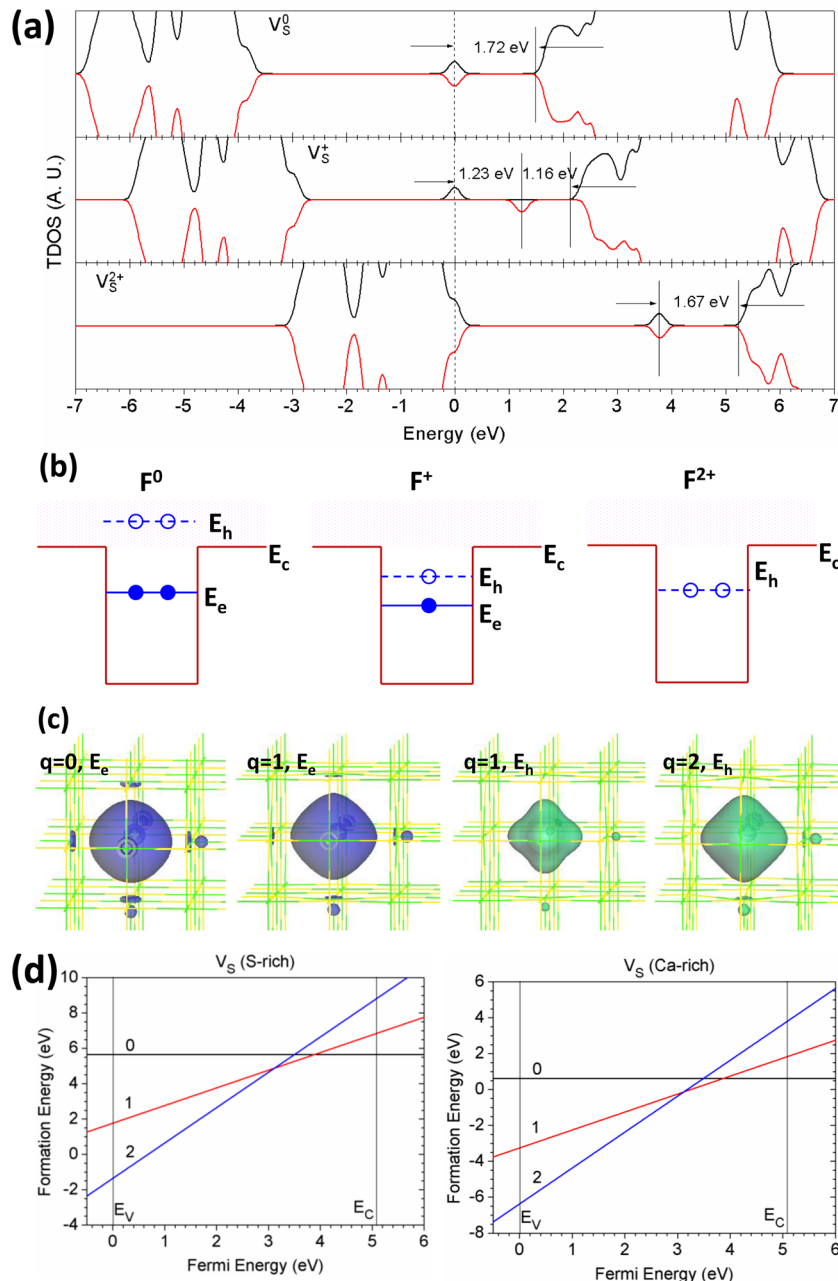


Figure 3. (a) TDOSs of V_S in neutral (V_S^0), singly positive (V_S^+), and doubly positive (V_S^{2+}) states. The dashed line denotes the highest occupied level for electrons. (b) Schematic single particle level of electron and hole levels for describing the F center defects. (c) Localized electron and hole orbitals at the relaxed V_S sites (Ca = green, S = yellow). (d) Formation energy of V_S under S- and Ca-rich chemical potential limits.

The localization of the orbitals are more evident than the neutral S_i site. While for the doubly negative S_i^{2-} , the relaxed structure is totally different. It sits in the center of a local cubic motif of CaS. The local tetrahedral bonding is pushing the neighboring S ions out of the local cubic motifs at the S_i^{2-} sites, as shown in Figure 4b.

The S_i in CaS is a negative- U_{eff} defect center at the transition state of (-2/0) with -1.26 eV for U_{eff} . This means the chemical reaction process for $2S_i^- \rightarrow S_i^0 + S_i^{2-}$ is an exothermal process. The electron spin resonance (ESR) measurement would find a very low density of S_i^- defect since there are only S_i^0 and S_i^{2-} stably existing in the lattice. The energy cost of these defect formations can be compensated by the local lattice distortions.

We see from Figure 4c, under the S-rich potential limit, that the S_i^0 has an energy of 2.06 eV to form in the CaS lattice, while it

is 6.23 eV for S_i^- under the S-rich limit. The S_i^- has similar trap levels in TDOS shown in Figure 4a, while the formation energy (Figure 4c) shows a very low possibility for S_i^- to singly form in the lattice. This is consistent with our deduced results from the negative- U_{eff} for the (-2/0) state.

Ca Vacancy (V_{Ca}). The V_{Ca} in CaS left two localized holes in the lattice staying at neighboring S sites. We see in Figure 5a that there are two localized single particle levels close in the band gap with 2.18 eV below the CBM and 2.83 eV higher than VBM, which are deep levels. The current calculations are able to reflect that the two holes are trapped at the two nearby S sites, as shown in Figure 5b.

For the singly negative Ca vacancy (V_{Ca}^-), there is only one localized hole left within the band gap, with the trap level of

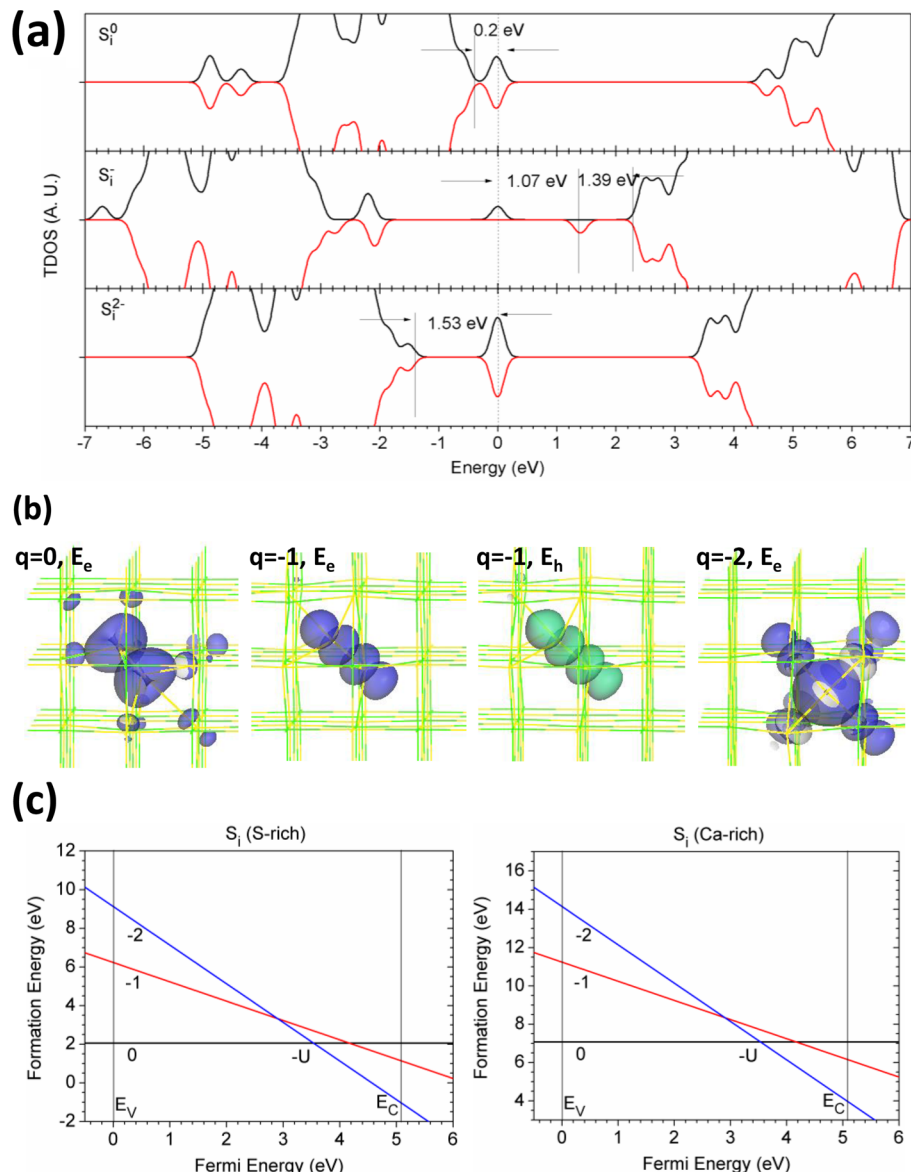


Figure 4. (a) TDOSs of S_i in neutral (S_i^0), singly negative (S_i^-), and doubly negative (S_i^{2-}) states. The dashed line denotes the highest occupied level for electrons. (b) Localized electron and hole orbitals at the relaxed S_i sites (Ca = green, S = yellow). (c) Formation energy of S_i under S- and Ca-rich chemical potential limits. The “ $-U$ ” denotes the negative- U_{eff} center for S_i at the $(-2/0)$ state.

2.18 eV unchanged. For the doubly negative V_{Ca}^{2-} site in CaS, there is no trap level in the band gap as no holes were left in the lattice. We also find from the partial density of states (PDOS) that the local trap states are induced by the local p-orbitals. These holes are localized on p-orbitals and lined up along the z-axis of S sites in CaS, as shown in Figure 5b.

From Figure 5c, the V_{Ca} is a positive- U_{eff} defect, which is about 0.14 eV. The $(-/0)$ shows an acceptor feature with 0.57 eV higher than the VBM. The difference of this energy level from the single particle trap level arises because the $(-/0)$ is the thermal ionization energy for the charge state varies from -1 to 0 , while the single particle level is the electron/holes occupation energy level in the band gap. The V_{Ca}^0 in CaS takes 2.74 and 7.76 eV to form under the S-rich and Ca-rich potential limits, respectively.

Ca Interstitial (Ca_i). The excess Ca in CaS (Ca_i) carries donor-like electrons. The neighboring S will form strong hybridized bonds to the Ca_i . We see from Figure 6a, that the donor-like level is 0.4 eV below the CBM for the Ca_i^0 with two

electrons, while it at a 0.3 eV level below the CBM for the singly positive Ca_i^+ with one electron occupancy. The doubly positive Ca_i^{2+} does not show any trap levels within the band gap. From Figure 6b, we see that the Ca_i^0 actually has two spin-up d_{z^2} -like electrons localized at the Ca_i^0 . This shows that the interstitial Ca with $3d^\delta 4s^{2-\delta}$ ($\delta > 0$) in the CaS lattice is actually donating its two electrons localized on d orbitals. For the Ca_i^+ , the localized orbital is strongly hybridized between d_{yz} and p orbitals (from S sites).

Figure 6c shows the formation energies of the Ca_i in $0, +1$, and $+2$ charge states with different chemical potential limits. We see that the transition levels of both $(+2/+1)$ and $(+1/0)$ states are in fact entering into the conduction band with about 0.4 eV. We also find that there is a positive- U_{eff} of 0.21 eV. For the neutral state, the Ca_i is energetically unfavorable in the CaS lattice since the formation energy is 12.47 and 7.46 eV at the S-rich and Ca-rich limits, respectively. For the Ca_i^+ , the formation energy turns down to the 6.90 and 1.88 eV at the S-rich and Ca-rich

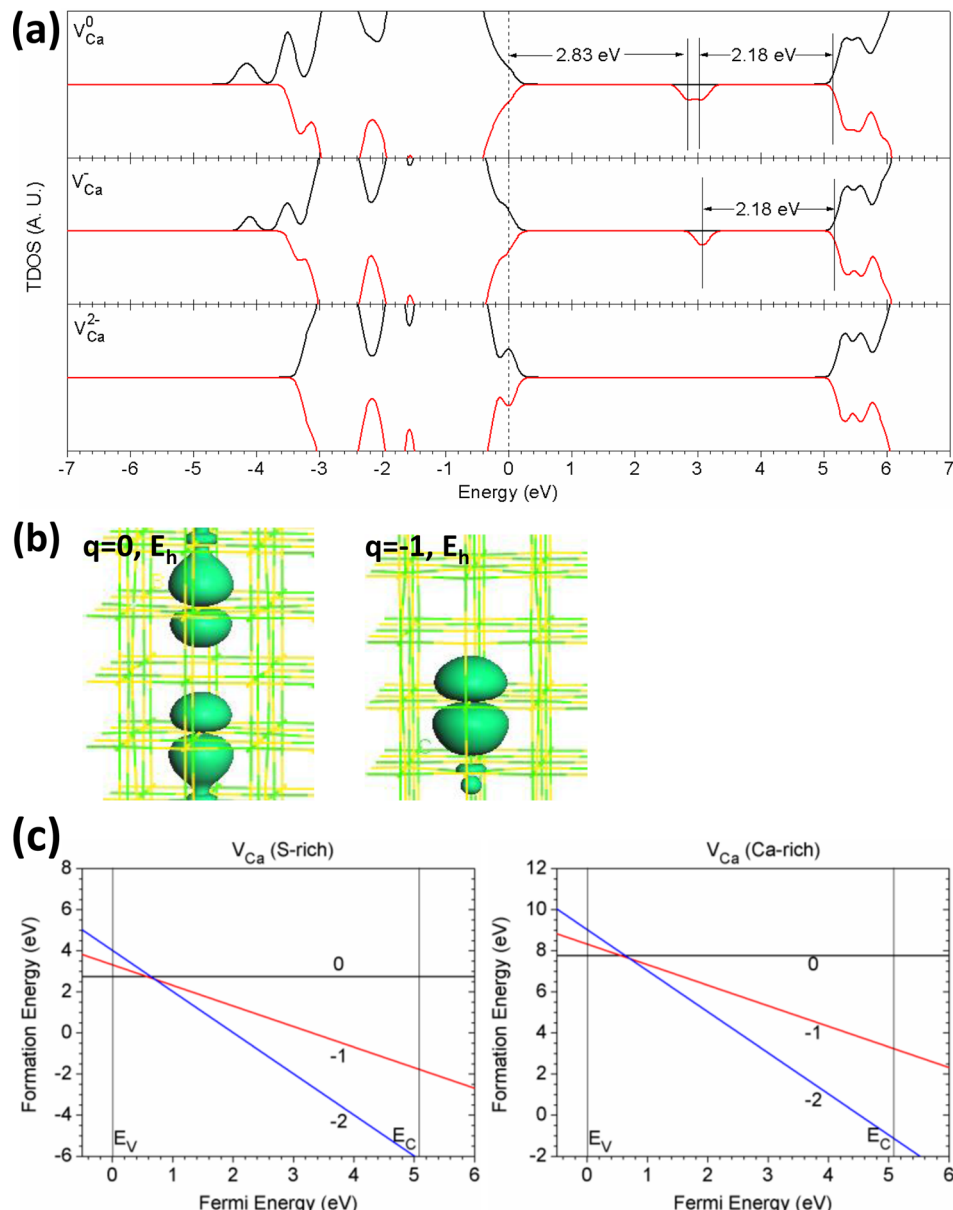


Figure 5. (a) TDOSs of V_{Ca} in neutral (V_{Ca}^0), singly negative (V_{Ca}^-), and doubly negative (V_{Ca}^{2-}) states. The dashed line denotes the highest occupied level for electrons. (b) Localized electron and hole orbitals at the relaxed V_{Ca} sites (Ca = green; S = yellow). (c) Formation energy of V_{Ca} under S- and Ca-rich chemical potential limits, showing a “+ U_{eff} ” defect with a shallow acceptor-trap feature.

limits, while it is still unknown for experiments that actualize the Ca^+ injection.

Frenkel Defects. The Frenkel defect denotes the escape of one ion from the original site that is trapped in the lattice, which is a complex of vacancy and interstitial space of the same ion. The Ca Frenkel defect we say is c-Fr, which means the cation is related. The S Frenkel is given as a-Fr showing that it is anion related. We first look at the a-Fr defect pair since the anion related defect like vacancy (V_S) and interstitial (S_i) usually induced ground state s-like electron trap level and excited state d-like hole trap level.

For the neutral a-Fr defect, Figure 7a shows that the TDOS has an ferromagnetic (FM) feature. The $V_S + S_i$ induces a p- π like band which is about 0.6 eV higher than the VBM, induced by the excess 3p electrons of S_i , and those p- π electron localized along the S-S bond formed by the S_i induced lattice distortions, as shown in Figure 7b. The deep electron trap level is 2.38 eV below

the CBM showing a deep donor-like state devoted by the V_S site with spin-up state. Another deep donor-like level with spin-down state about 2.25 eV below the CBM is contributed by the S_i site with a p- π like orbital along the S-S bond direction, as shown in Figure 7a and b. We also found the two pairs with spin-up electron and spin-down hole states. The energies between the two pair states are 1.24 and 1.38 eV, as shown in Figure 7a. From the charge orbital analysis, the pair-states with 1.24 eV is contributed by V_S , and the pair-states with 1.38 eV is given by S_i .

The formation energy study shows that the a-Fr defect has 8.22 eV per pair defect, which means 4.11 eV for each point defect. We show the formation energies of the a-Fr with charge states of -1, 0, and +1. We see the a-Fr is a negative- U_{eff} defect center with an energy of -1.48 eV for the exothermal process: $2(\text{a-Fr})^0 \rightarrow (\text{a-Fr})^+ + (\text{a-Fr})^-$. The transition state of (\mp) stays at 3.61 eV in the band gap and shows that the thermal ionization energy of a-Fr(\mp) defect pair is about 1.52 eV below the CBM.

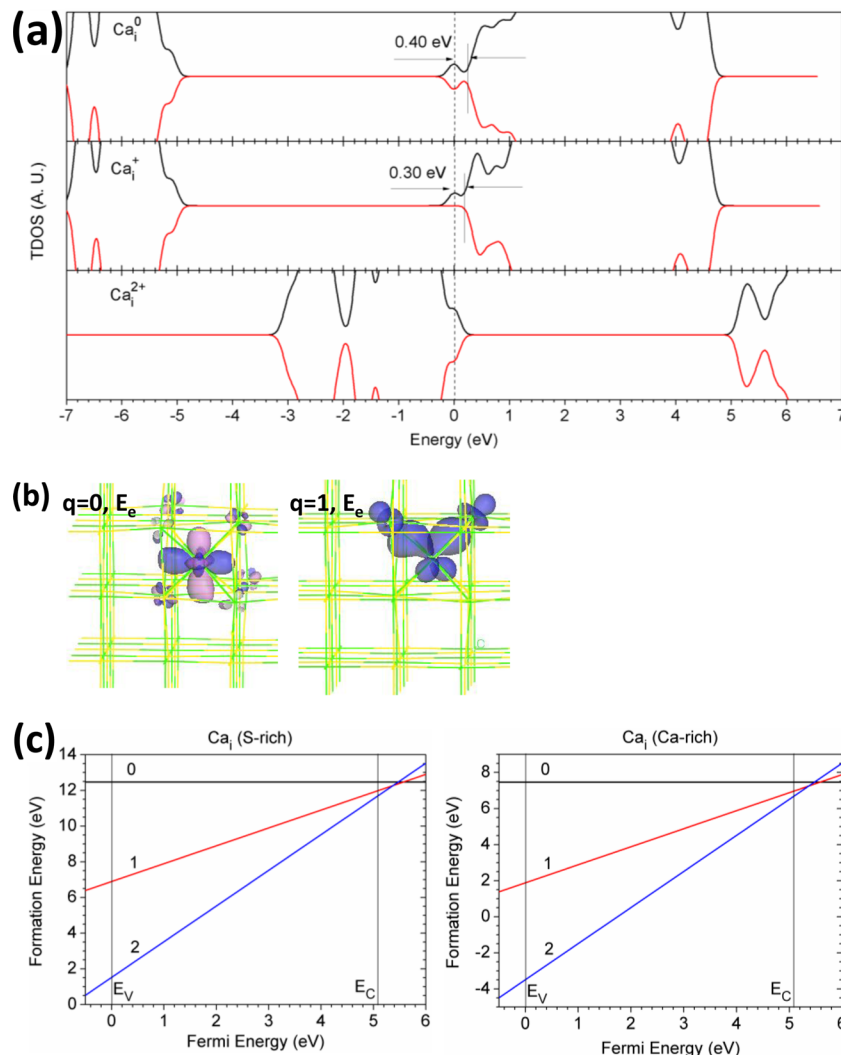


Figure 6. (a) TDOSs of Ca_i in neutral (Ca_i^0), singly positive (Ca_i^+), and doubly positive (Ca_i^{2+}) states. The dashed line denotes the highest occupied level for electrons. (b) Localized electron orbitals at the relaxed Ca_i sites, showing a hybridized d-orbital feature (Ca = green, S = yellow). (c) Formation energy of Ca_i under S- and Ca-rich chemical potential limits, showing a “ $+U_{\text{eff}}$ ” defect with a shallow donor-trap feature.

Therefore, the realistic a-Fr defect pair exists as a-Fr^(±) with a formation energy of 3.74 eV per defect site, which is from the formation energy of the a-Fr⁰ deduced by $|U_{\text{eff}}|/2$, as learned from Figure 7b.

Schottky Defects. The Schottky defect in CaS is formed by the Ca and S monovacancies ($\text{V}_{\text{Ca}} + \text{V}_S$). In this type of defect, the two electrons left by V_S at the Schottky defect site are neutralized by the two holes induced by V_{Ca} . Compared to the Frenkel defect pair, the Schottky defect pair has been found to be dominant in ionic compounds like alkaline-earth sulfides and other alkali-halides by Pandey et al.^{47–49}

Figure 8a shows the TDOS of the Schottky defect pair in CaS within different charge states, $-1, 0 + 1$. The neutral state of such a defect gives only the localized hole trap levels with 1.30 eV below the CBM, contributed by the d-orbitals of 5 nearby Ca sites. For the singly positive state, there are three localized holes within the band gap where two of them are spin-up and down in the same level. The energy intervals of the two trap level is 0.91 eV. The singly negative state has one localized electron and one localized hole in the band gap with the energy of 1.26 eV between these two states, and the localized hole state is 1.09 eV below the CBM.

We see from Figure 8b that the localized electron and hole state wave functions are similar to the case of V_S^+ discussed in previous content, which are all contributed by the d-orbitals of first neighboring Ca sites.

From the formation energy calculation, the Schottky defect pair has 3.01 eV per pair in neutral state, which means 1.51 eV per defect site. It is 2.23 eV lower than the a-Fr^(±) defect pair discussed above. However, the Schottky defect pair has positive- U_{eff} of 1.69 eV for the process: $2(\text{STK})^0 \rightarrow (\text{STK})^+ + (\text{STK})^-$.

Eu and Dy Doping Levels in CaS. Experiments reported that the Eu doping in CaS contributes optical transition with a gap of about 1.90 eV (650 nm) for red luminescence, which is mainly contributed from ${}^6\text{P}_{7/2}$ to ${}^8\text{S}_{7/2}$.⁷ This denotes the valence states from excited $4f^65d^1$ (T_{2g}) to ground state $4f^7$ of the Eu ions. Thus, it is necessary to interpret the energy levels for 4f and 5d orbitals of Eu ions in CaS. We have investigated Eu and Dy substitution doping in CaS with 4 different charge states ($0, +1, +2$, and $+3$). The reason is that the Ca ion radius is 0.99 Å very close to the 1.07 Å for Eu³⁺ and 1.05 for Dy³⁺.

The neutral Eu (Eu⁰) in the CaS lattice does not contribute any gap states that potentially form levels for optical transitions of luminescence, which has 4.6 eV of separation between

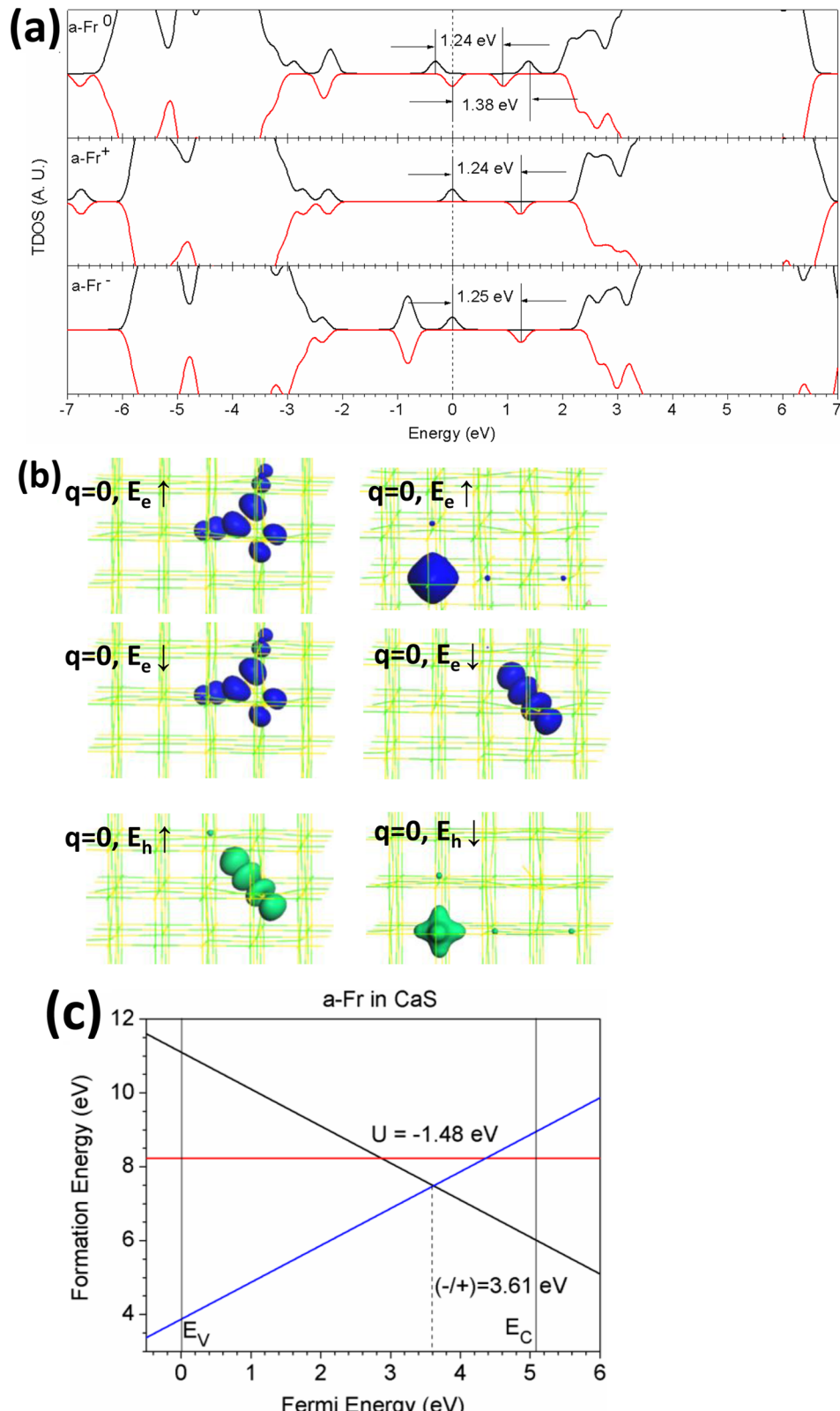


Figure 7. (a) TDOSs of a-Fr in neutral ($a\text{-Fr}^0$), singly positive ($a\text{-Fr}^+$), and singly negative ($a\text{-Fr}^-$) states. The dashed line denotes the highest occupied level for electrons. (b) Localized electron orbitals at the relaxed $a\text{-Fr}^0$ sites, ($\text{Ca} = \text{green}$, $\text{S} = \text{yellow}$). (c) Formation energy of $a\text{-Fr}^0$ showing a “ $-U_{\text{eff}}$ ” defect with transition energy of 3.61 eV for the state (\mp) .

occupied 4f to empty 5d levels (Figure 9a). The two filled 4f states stay 0.03 and 0.30 eV below VBM. The left dashed lines at the 0 eV denote the highest occupied levels for electrons, and the right dashed lines at higher energy (~5 eV) represent the

conduction band edge. According to the on-site d orbital projected density of states (PDOS) on the Eu ion, the d-up and -down electrons near the CBM overlap with the d orbitals of other nearby Ca sites for Eu^0 in CaS, while the spin unpaired

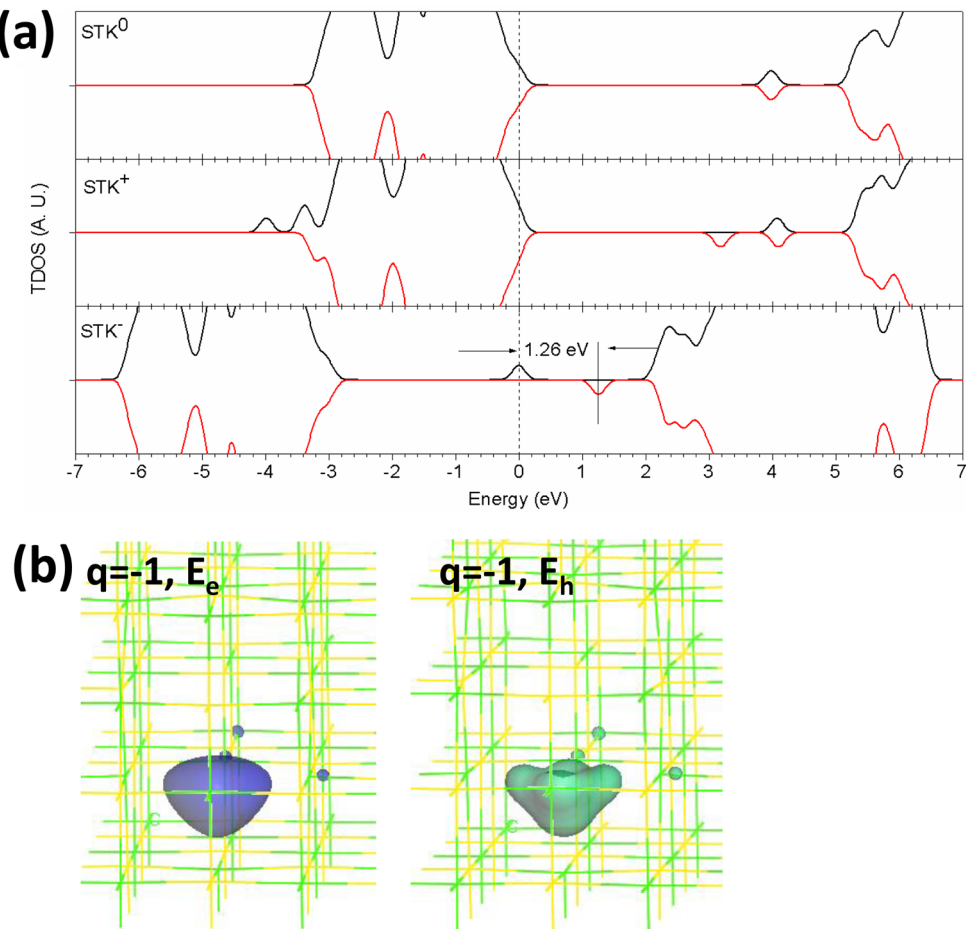


Figure 8. (a) TDOSs of the Schottky defect pair in neutral (STK^0), singly positive (STK^+), and singly negative (STK^-) states. The dashed line denotes the highest occupied level for electrons. (b) Localized electron and hole orbitals at the relaxed STK^- sites (Ca = green, S = yellow).

d electrons for the Figure 9a for Eu^+ , Eu^{2+} , and Eu^{3+} are dominantly contributed by the Eu positive ions. As shown above, the position of the 5d bands is nearly overlapped with the CBM of the host, which means the electrons transferred to 5d levels may easily be transported in the lattice through the delocalized conduction band.

For the PDOS of the f-orbital, based on the calculation of the area of the PDOS spectra for the f-orbital, the number of f-electrons on the Eu^0 and Eu^+ sites is 6.9 and 6.2 e, respectively. They stay at the VBM and about 6 eV below the VBM, respectively. On the basis of the Mulliken analysis, the total valence electron occupations on all valence orbitals for the Eu^0 and Eu^+ are 16.66 and 16.54, with a charge of +0.34 e and +0.46 e, respectively. For the Eu^{2+} in CaS, the occupied 4f levels (twin-peak) with 5–6 eV below the VBM (0 eV) shows the area weight of 7.06 electrons located from -5.3 eV to -6.4 eV, while there is only one empty 4f level within the band gap area with 2.1 eV above 0 eV, which acts like antibonding orbitals for the localized holes. The level at 4.5 eV above VBM (0 eV) is at the 5d level given by the 5d orbital of Eu^{2+} in the middle panel of Figure 9a. For the Eu^{3+} in CaS, the occupied 4f levels have split into three peaks with 6–8 eV below the VBM. The area weight of the occupied 4f levels show 6.33 electrons localized from -6.0 eV to -7.8 eV. There is also one empty 4f level within the band gap area with 1.67 eV above the VBM and 0.6 eV lower than the case of Eu^{2+} .

Theoretically, for the Eu^{2+} in the solids, the ground state has a half-filled $4f^7$ shell with all the spins aligned, and the excited state has the $4f^65d^1$ structure with the six 4f electrons spin aligned leaving one empty 4f state in the band gap. For Eu^{3+} , it has six 4f electrons occupied in the orbitals. We can see that the occupied 4f electrons for Eu^{2+} and Eu^{3+} are not exactly showing the 7 and 6 electrons, respectively. This arises because of an issue as to whether pseudopotential-based DFT can describe the $4f^N$ spectra of lanthanides. The pseudopotential in DFT cannot distinguish between $4f^N$ and $4f^{N-1}$ with 5d very evident to be even the norm-conserving type. The valence charge density does exhibit considerably distinguished charge, especially between the 5d–6s orbitals. Although the nonlinear core correction helps to screen the core–valence charge density,³⁴ for even heavier lanthanide elements, the 4f orbital is still difficult to distinguish energetically within valence charge densities.

The Eu^+ ion in CaS has one 4f state localized in the band gap of the CaS area, the 5d level showing spin polarized with ferromagnetic behavior near the conduction band edge. The 4f level has an energy of about 2.30 eV (measured from edge-to-edge) lower than the nearest 5d level (spin-up), which is 0.4 eV larger than the required 1.90 eV emission (650 nm). The 5d level (spin-up) has a separation of 0.94 eV between itself and CBM of CaS, which does not correspond to the experimental value very well.⁷ Thus, the Eu^+ is not a suitable activator center. In such singly positive state Eu doping in CaS, the 4f and 5d levels are all

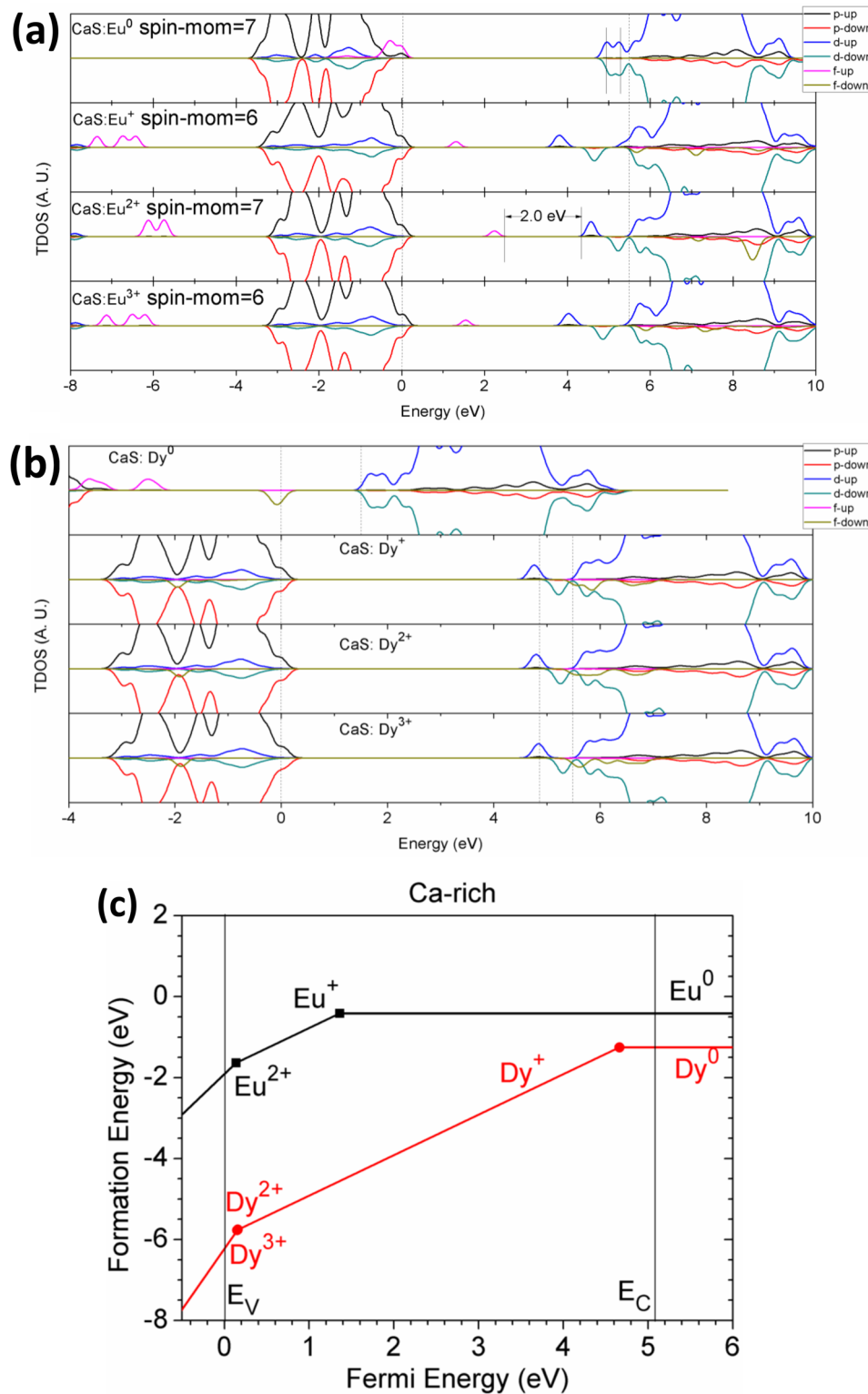


Figure 9. (a and b) TDOSs of Eu and Dy doping in CaS within different charge states. The dashed lines on the left at 0 eV denote the highest occupied levels for electrons, and the dashed lines on the right at higher energy (~ 5 eV) represent the conduction band edge. (c) Formation energy of Eu and Dy doping in CaS.

empty states localized within the band gap of CaS, while the filled 4f states are 6.2, 6.6, and 7.6 eV below the VBM, respectively.

From the aspect of electronic eigenvalues in the orbitals, we find that 4f–5d transition intervals of Eu²⁺ and Eu³⁺ stay in the band gap of CaS are 1.85 and 2.23 eV, respectively. The 4f empty level of Eu³⁺ has a 0.56 eV lower value than Eu²⁺, and the 5d level

has a 0.42 eV lower value. The highest 5d level of Eu²⁺ is close to the CBM with only 0.04 eV difference. This leads to an evidence of capable accommodation of delocalized transporting electrons by Eu²⁺, and a suitable transition gap size (1.85 eV by us) denotes the experimental 650 nm red-emission.⁷ Thus, only Eu²⁺ is responsible for the activator consistent to experiments.^{7,16}

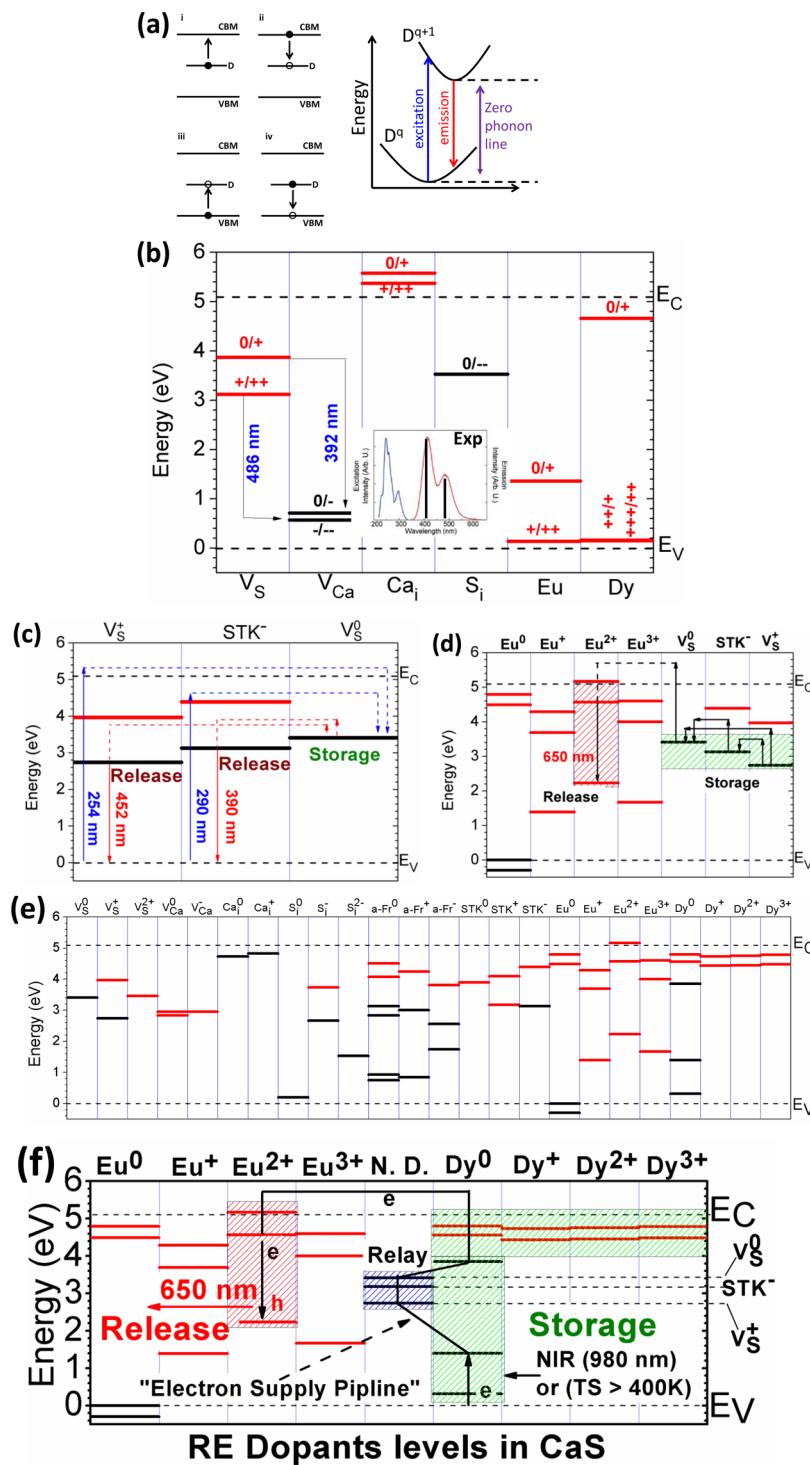


Figure 10. (a) Summary of four simplified optical transitions. (b) Thermodynamic transition levels of different charge states of the intrinsic defects and RE ion doping in CaS (RE = Eu and Dy). The insert shows experimental ordinary persistent luminescence induced by intrinsic defects of undoped CaS. The red line denotes the donor type transition level, and the black line shows the acceptor level. (c) Storage and release levels of undoped CaS for persistent luminescence (excitation = blue vertical solid and horizontal dashed lines, emission = red vertical solid and horizontal dashed lines, empty states = red horizontal solid lines, and filled states = black horizontal solid lines). (d) Storage and release levels of Eu doped CaS for persistent luminescence. (e) Summarized single-particle levels of intrinsic defects and RE dopants in CaS with different charge states (RE = Eu and Dy, empty states = red, and filled states = black). (f) Native defects (N. D.) and dopant level related luminescence mechanism. The black bent line denotes the lengthened optical transition path for persistent luminescence, which is an intact “supply line” for electron transport.

In addition, we verified the energy levels between 4f and 5d of Eu^{2+} doping in CaS by ab initio prediction, particularly the self-consistent determination of the 4f on-site Coulomb corrections.

From the aspect of binding energies of ions, we refer to a theoretical model on the vacuum referred binding energy (VRBE).^{7,50,51} The electronic binding energy of these three ion states (Eu^+ , Eu^{2+} , and Eu^{3+}) are very different according to the

obtained levels of vacuum referred binding energy (VRBE).^{7,50,51} We can confirm that the Eu²⁺ is more appropriate to be an activator in luminescence as the Eu³⁺ has stronger binding energy that cannot release the electrons easily to create 4f-based holes in the forbidden gap area upon the UV-254 nm excitation in the experiment.⁷

We find that the neutral state of Dy (Dy⁰) in CaS has three deep electron trap levels widely spread within the band gap area (Figure 9b), which are 0.31, 1.40, and 3.85 eV above the VBM. The highest occupied 4f level is 1.28 eV below the conduction band edge (or E_V +3.85 eV, E_V = VBM) which contributes a closer electron source level in CaS. The other two filled levels stay rather deep close to VBM that traps electrons securely as the storage center. The experiments reported that the trap levels that donated the electron were about 1.3 eV below the CBM in CaS for the persistent luminescence occurrence, which shows a very close value and correspondence to our calculated results (1.28 eV). The energy barrier of 1.3 eV for the electron excitation can be excited by 980 nm laser irradiation. This confirms the validity of the DFT+U for predicting the RE ions doping levels in the insulating materials such as CaS for persistent luminescence applications. Other states like Dy⁺, Dy²⁺, and Dy³⁺ have two shallow empty 5d states below the CBM with separations of 0.4 and 0.6 eV respectively. The filled 4f states of positive Dy ion are all below the VBM and split into three different levels, e.g., 1.88, 5.08, and 6.37 eV below the VBM for Dy³⁺, the difference of these three levels for Dy⁺ and Dy²⁺ is only about ± 0.04 eV. Consider the thermal dynamic transition levels, the Dy dopant has very low shallow donor transition level of (0+/+) with 0.5 eV below the CBM, compared to the deep donor level of Eu shown in Figure 9c.

Native Defects or Doping Levels Induced Luminescent Properties.

It is worth noting that the major prerequisite of persistent luminescence is how to deliver the ongoing electrons excited from the trap levels or even VBM, and recombine with holes at defect sites. It is also closely related to the major goal of lengthening the duration time of persistent luminescence. Before that, it is necessary to understand the optical transitions under the framework of DFT. It is basically divided into excitation and emission and with multiphonon or zero-phonon radiations for each emission.

Figure 10a shows the simplified optical mechanism of excitation and emission for a localized defect state. For the process of (i) and (iv), the charge state transitions are from q to q+1, while for (ii) and (iii) it is from q to q-1. The transition energy of the zero-phonon line (or E_{ZPL}) denotes the energy differences of the excited- and ground-state geometries at their equilibrium states. The E_{ZPL} actually corresponds to the energy difference between the thermodynamic transition level and the CBM, which may be the possible highest efficiency photoemission. Thus, we can determine the boundary of the whole optical excitation and emission processes with calculations of optical transition levels, and the specific peaks of emission spectra can be determined through the difference of the E_{ZPL} (i.e., difference of the thermodynamic transition levels). These mechanisms and related equations for calculating the optical transition levels have been summarized by Lany and Zunger.⁴²

The luminescence experiment shows the undoped CaS has blue broad band emissions between the range of 350 and 550 nm with two peaks at about 400 and 490 nm, respectively,⁷ which are stimulated by NIR ranged irradiation. Experimental explanation attributes this to the presence of the intrinsic defect as well as the impurities of Na⁺ during the synthesis assisted by Na₂S. From our

calculations on thermodynamic transition levels of intrinsic defects, we see that the arrow indicates in Figure 10b a dominant contribution to the emission state by (1) singly charged donor–acceptor recombination: (0+/+) → (-/-) with 392 nm and (2) doubly charged donor to acceptor recombination (+/++) → (-/-) with 486 nm.

It is necessary to understand the role of native defect levels in the undoped CaS according to our calculations and available experimental reported data. We summarized the optical (vertical) transition levels of the native defects in undoped CaS in Table 1 that corresponds to the experimental spectra⁷ very

Table 1. Calculated Optical Transition Levels of the Native Defects in CaS That Correspond to the Extent of Spectra Measured by Experiment.^{7,16a}

defects (D)	excitation (opt. absorption)			
	charge states transitions	optical transition level (eV)	wavelength (nm)	path
V _S	0/-1	5.00	248	VBM→D
	+1/0	4.22	294	VBM→D
	+2/+1	3.58	346	VBM→D
V _{Ca}	-2/-1	5.49	226	VBM→D
C _{Ai}	+1/0	5.53	224	VBM→D
STK	0/-1	3.24	383	VBM→D
	0/+1	4.83	257	D→CBM
photo-emission				
defects (D)	charge states transitions	optical transition level (eV)	wavelength (nm)	path
	+1/+2	-3.58	-346	D→VBM
	0/+1	-3.51	-353	D→VBM
STK	-1/0	-2.16	-574	D→VBM

^aThe optical transition levels of the defects that mismatch the experimental spectra^{7,16} are not listed in the table here.

well. The other defects mismatched the experimental excitation and emission spectra,⁷ which are not listed. Compared to our calculations with experimental data, the defects listed in Table 1 are confirmed as the possible contributions in luminescence by optical transitions. We see from Table 1 that for the process of the excitations, these defects act as intermediate to accommodate the excited electrons that are pumped out by photoexcitations. Meanwhile, the defect formation energies (costs) should also be taken into account, as summarized in Table 2. Thus, the standalone V_{Ca} and C_{Ai} are excluded to optical transitions as their high formation energies, and the V_S and STK defects stay for optical transition process. For the process of photoemission, both V_S and STK provide the source levels to put electrons back to the VBM to recombine with the holes, which also correspond to our analysis of defect formation energies.

Regarding the path of optical transition during the persistent luminescence, it is vital to determine the single-particle levels of native point defects and dopants in each charge state. Figure 10c shows the path of the persistent luminescence. The V_S⁰ acts as the storage center to accommodate the excited electrons at its level. The excitations of electrons from VBM are illustrated. The experimental UV irradiation of 254 nm is about 4.88 eV close to the extent of CBM that pumps electrons from VBM to the V_S⁰ site via CBM, which are stored (or trapped) at the V_S⁰ site. Another excitation path is found via the empty state of the STK⁻ site with an excitation energy of 4.27 eV (290 nm) from the experiment.⁷ The empty state of STK⁻ is about 4.39 eV according to our calculation shown in Figure 10c, close to

Table 2. Summary of Formation Energies of Native Point Defects in Different Charge States in CaS under Both S-Rich and Ca-Rich Chemical Potential Limits (Unit: eV)^a

	S-rich	Ca-rich		S-rich	Ca-rich		S-rich	Ca-rich
V _S	0	5.63	0.62	V _{Ca}	0	2.74	7.76	a-Fr
	+1	1.76	-3.25		-1	3.31	8.32	0
	+2	-1.36	-6.37		-2	4.02	9.03	+1
S _i	0	2.06	7.07	Ca _i	0	12.47	7.46	STK
	-1	6.23	11.24		+1	6.90	1.88	0
	-2	9.13	14.14		+2	1.53	-3.49	+1

^aNote, the a-Fr and STK are both pair defects; their formation energies should be divided by two as occurrence per defect when used for discussion, and the neutral a-Fr pair (a-Fr⁰) should be also corrected by deducing |U_{eff}|/2 (U_{eff} < 0).

experimental data with only a difference of 0.08 eV. The role of V_S⁺ can be either trap level for electron storage or release center for photoemission, which is the prominent F⁺ center of ionic crystals. Its highest trap level is 1.16 eV below the CBM and very close to the reported value of 1.11 eV from the thermally stimulated luminescence (TSL) experiment.⁷ The V_S⁰ will decay the electron back to the V_S⁺ state due to the positive U_{eff} discussed previously in section 3.2 or transfer the electron to the filled state of STK⁻ with a small energy barrier of about 0.2 eV. The emission wavelength is calculated as 390 and 452 nm through STK⁻ and V_S⁺ sites, respectively. The difference between calculated 452 nm and experimental 490 nm may be due to the error of measurement between peak-to-peak and edge-to-edge. The mechanism discussed above corresponds to the ordinary persistent luminescence as illustrated in the Figure 1a.

Consider the case of CaS doped with Eu (CaS/Eu²⁺). The luminescence spectra from the experiment⁷ show two emission peaks due to the host native defects recombination and optical dipole transition between 4f⁷↔4f⁶5d¹ (1.90 eV) of Eu²⁺. The emission by the native defects in the host has been illustrated in Figure 10c. According to Figure 10c, the V_S⁰ is the storage center, and both V_S⁺ and STK⁻ are the release centers for the blue persistent luminescence in undoped CaS. However, the roles of these defects have all been redirected into the storage center dominantly for 650 nm persistent luminescence of Er²⁺ doped CaS, as shown in Figure 10d. We deduce that this may be the reason for the reported duration of this red persistent luminescence (CaS: Eu²⁺) being about three times longer than the case of the undoped CaS (12 s under power of 75 mW).⁷ The previous blue persistent luminescence still remained since it is the intrinsic optical property observed as a lower emission peak (400–500 nm) in the luminescence experiment^{7,16} of CaS/Eu²⁺. Therefore, the native defects in CaS/Eu²⁺ are the dominant storage centers, and the V_S⁺ is the deepest storage level with 2.39 eV below the CBM. The native defects and Eu dopant are not independent; simply increasing the Eu dopant concentration cannot increase the intensity of luminescence as found in the experiment,¹⁶ where reported the highest intensity was only 0.02 mol % of Eu²⁺ in CaS.

Matsuzawa et al. proposed the “hole-transfer mechanism” to explain the role of Eu ion for persistent luminescence in SrAl₂O₄ or similar insulators² with induction of unique valence state of Eu (e.g., Eu⁺), while other experiments argue that there are no valence changes during the whole process of stimulation and luminescence.^{17–19} From our calculation, we find that there is no need to argue and determine the existence of Eu⁺, as the 4f–5d transition gap is too large and the 5d level too deep to accommodate the delocalized transporting electrons from CBM.

We turn to look at the role of Dy dopant and the interplay effect by the native defects in the persistent luminescence of

CaS: Eu²⁺. We found that the shallow donor transition level of Dy corresponds to the observation from experiments that Dy not only contributes the deeper occupied 4f level to store the electron for extending the time but also gives shallow donor transition levels to enable the thermal or near-infrared stimulation to relax the electron into the conduction band easily. As summarized in Figure 10e, the electron trap levels contributed by Dy widely spread the band gap area. We see that there are three filled states of Dy⁰ in CaS: 0.31, 1.40, and 3.85 eV above the VBM. They can be possible deep trap level storage sites of the excited electrons, but the question is, upon the charge transfer occurring after doping, how can these trap levels with wide gaps (~2.45 eV) perform both storage and photo-stimulated luminescence (NIR 980 nm, 1.3 eV) well? In the recent mechanistic study of the persistent luminescence of CaAl₂O₄ doped by Eu and Nd,¹⁵ Zeng et al. proposed that the second RE dopant like Nd contributes the levels of 0.55–1.45 eV below the CBM to vastly extend the luminescence time (>19 h), and the calculated levels are close to the experimental 1.2 eV from their work. As they proposed, the second RE dopant like Nd contributes not only the deep trap levels but also the charge carriers. Inspired by their model, here in the persistent luminescence of CaS doped by Eu and Dy, all the deep electron trap levels of Dy are active and act as a storage center for PSL conforming only with help of the native defects like V_S⁰, V_S⁺, and STK⁻ as shown in Figure 10f. This deduction shows accordance with experiments^{7,16} that the persistent luminescence time is over 100 times longer than the case of up-doped CaS with a rather small concentration of Dy dopant (0.002 mol %).

Therefore, if we line up the electron levels of both Dy dopant and native defects of host, we see from Figure 10f that the native point defects like V_S⁰, V_S⁺, and STK⁻ play a key cooperative role as a relay center that transfers the ongoing electron continuously into CBM with energy intervals lower than 1.3 eV. Meanwhile, the Dy acts not just only on the deep trap levels and carriers supply centers, more importantly, it aligns with native defect levels by a mutually cooperative way in order to drain the electrons up from VBM continuously, which can be easily stimulated by NIR 980 nm, as elucidated in Figure 10f. The black fold line denotes the lengthened optical transition path for persistent luminescence, which is an intact “supply line” for electrons transport.

We need to pay some attention to the selection-rule especially on the parity-selection-rule for this optical transition. We realized that the electron transport by the optical excitation along the 4f^N↔4f^N transition is maybe electrical-dipole forbidden but only be possible if the octahedral (centrosymmetric or inversion) symmetry of Dy dopant site is broken through the local lattice distortions or 4f-orbital wave function overlap with nearby 3p orbitals of S sites in CaS lattice. Another route is to transfer

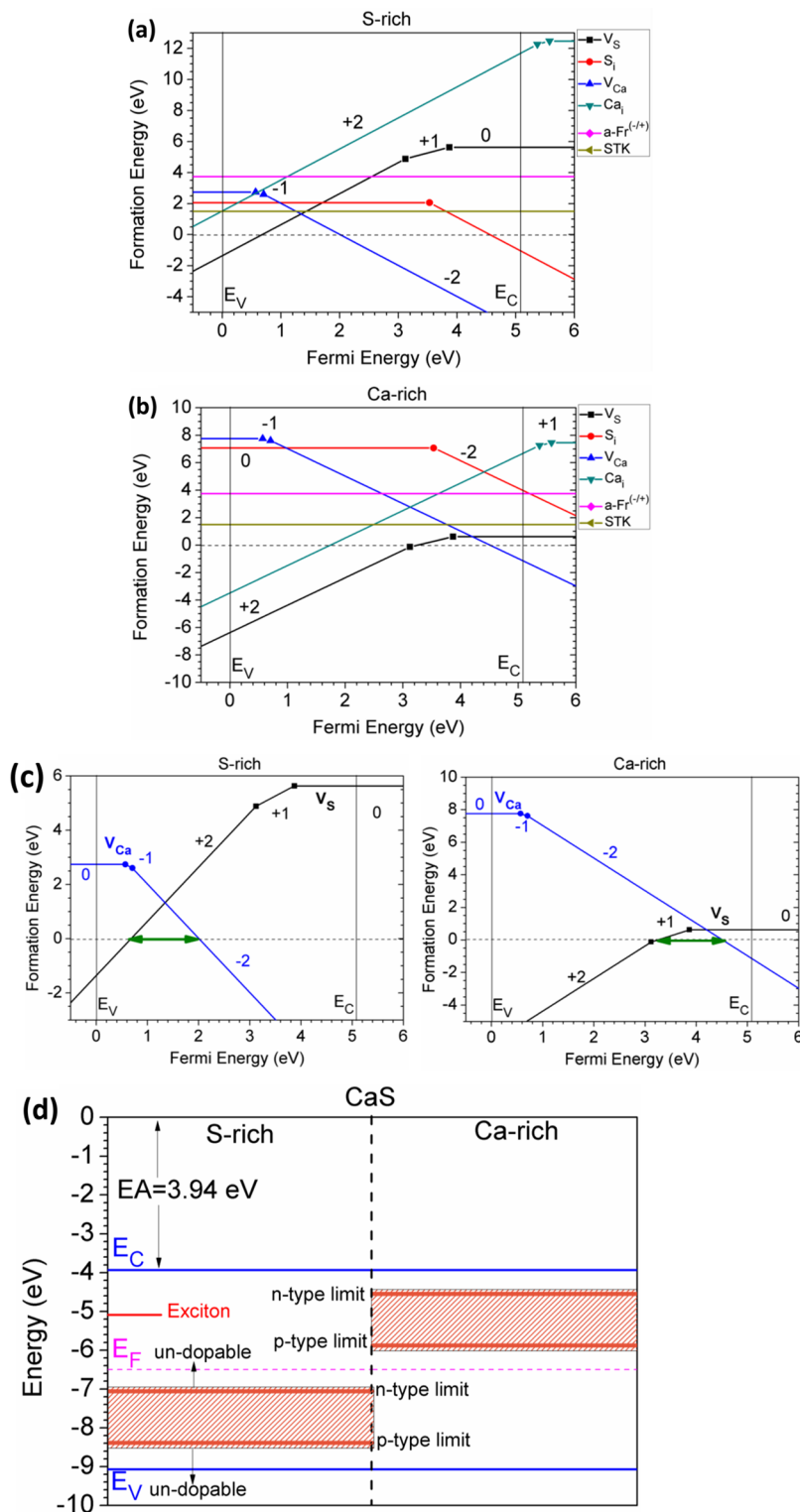


Figure 11. Summary of the native point defects in CaS under S-rich (a) and Ca-rich (b) chemical potential limits. (c) The doping limit energy determined by the native point defect formation energies (V_S and V_{Ca} in CaS); the green arrow indicates the dopable range. (d) Schematic band diagram of valence and conduction bands (E_V and E_C), ideal Fermi level (E_F), doping limit (shaded area), exciton level by native point defects, and electron affinity energy (EA), against the vacuum level (0 eV).

electrons following the parity-selection rule. Both of these are approachable and observable through our DFT calculations, e.g., from Figure 9b we can see from the TDOS that the lowest occupied 4f electron trap levels has evident overlap in 3p orbitals of S sites. This means the electron with an even parity due to this

overlap at the lowest occupied 4f levels can be excited to the second 4f level with odd parity, then transfer to the third 4f level via intermediate native point defect levels from different sites and finally to the 5d levels that are close to the CBM with even parity. Recalling the model explained by Zeng et al.,⁷ the significant

progress of this work is that we extensively detailed that model if the second dopant acts as both charge carrier supplying center and deep trap center, with considerations of many factors of restrictions and promotions.

This is actually a possible cooperative up-conversion persistent luminescence. Such up-converted features depend on the ladder-like electron trap levels aligned in the band gap area of host CaS. Interestingly, these ladder-like trap levels are not derived from the up-converted lanthanide ions like Eu or Dy. It is actually an indispensable cooperative contribution from native point defects (V_S^0 , V_S^+ , and STK^-) and Dy in the CaS. To understand this in an easier way, the band gap of the host CaS is calculated as 5.13 eV, which would require at-least a four-photon (each photon with 980 nm, ~1.3 eV) up-conversion. Now a three-photon level has already been preconditioned when the Dy^{3+} turns to neutral Dy^0 as obtained by three excited electrons at the initial stage of UV excitation from VBM; the electrons will store in terms of the trap levels as shown in Figure 10f. The native point defect levels will fill in the gap of the Dy electron trap levels to line-up an intact pipeline for electron transport back to the delocalized conduction band when it is 980 nm photo-stimulated. Another similar up-converted persistent luminescence has been found from the experiment by Liu et al.⁸ Our model is also consistent if we combine the empirical VRBE level analysis with consideration of excited states;⁷ the intrinsic defect levels can bridge the gap of the excited states of the Dy^{3+} to continuously transport the excited electrons up from the lowest excited states to the conduction band via the native defect states like V_S^0 , V_S^+ , and STK^- .

We further deduce that the luminescence through the electron transition from the 5d to 4f level of the Eu activator is sourced from donor trap centers that contain a large amount of electron carriers. This may come into a comparison as to which one is more easily ionized to donate electrons, i.e., we need to confirm that the electrons are more easily contributed by the intrinsic donor trap defects in CaS or the dopant of Dy ion in CaS. Since the V_S^0 level is the highest electron trap level active as the intermediate, therefore we compared the difference of (0/+) thermodynamic transition levels between V_S and Dy in CaS as shown in Figure 10b. We see that the (0/+) thermodynamic transition level of V_S is at the 1.1 eV below the conduction band edge, which also can be seen from Figure 2d. This means that the (0/+) of V_S is sitting lower than the level contributed by the (0/+) of Dy dopant in CaS, where it is 0.5 eV below the CBM. This means that the electron goes into CBM more easily from the highest occupied level of Dy (3.85 eV in Figure 10f) than the V_S . Moreover, the (+2+) and (2+/3+) levels of Dy are even lower than the (+2+) level of V_S shown in Figure 10b. Thus, the native defect V_S is further confirmed as one of the crucial cooperative centers whose thermodynamic transition levels align between the levels of Dy.

As discussed above, we can use the calculated results to deduce that the Dy dopant contributed deeper trap levels in the CaS materials that can store the electron carriers with more evenly, wider and deeper range of levels distributed so that the decay-time of the persistent luminescence is prolonged. The related 980 nm photo-stimulated luminescence is actualized with the help of native defects like V_S^0 , V_S^+ , and STK^- as a relay center for a possible up-converted luminescence (Figure 10f). We further confirm this model with calculations with different charge states of the Dy doping in the CaS (0, +1, +2, and +3).

Doping Limit. Figure 11a and b summarizes the native point defects in both S-rich and Ca-rich limits discussed above, which

helps us to systematically analyze the doping in CaS using the concept of pinning energy rule. The pinning energy rule consists of n-type pinning energy and p-type pinning energy as elucidated by Robertson et al.⁵² As introduced, the key limitation for doping in CaS is native defect compensation. This occurs because the Fermi level (E_F) moves to a specific band edge that causes the spontaneous formation of compensating defects because the formation energy of the defect has fallen to zero at that E_F position. We see that, for the neutral charge state, V_S has the lowest formation energy in Ca-rich (S-poor) limit, as low as 0.62 eV. The neutral Schottky defect ($V_{Ca}+V_S$) has the second lowest formation energy of 1.51 eV per defect site, which presents another dominant defect existing in CaS.

We further discussed the doping limit energy determined by the native point defects of CaS. Figure 11c further plots the formation energy of the most stable charge state of the most stable donor-type and acceptor-type native defects for crystal CaS. It shows that the V_S^{2+} and V_{Ca}^{2-} are the most defects coexisting in CaS under both S-rich and Ca-rich limits. We first discussed the case of S-rich. If a donor is used to raise E_F toward the conduction band edge (CBM, or E_C in Figure), we must consider the formation energy of possible negatively charged compensating acceptors such as V_{Ca} or S_i . Figure 8a and b shows that the V_{Ca} is the more stable of these two defects and that the E_F moves to 2.01 eV for V_{Ca}^{2-} to form spontaneously. This energy is called the "n-type pinning energy" (or n-type limit) for donors.^{52,53}

However, if an acceptor dopant is used to shift the E_F to move lower in energy toward valence band edge E_V (or VBM), we must look at the formation energy of compensating donor defects such as V_S or Ca_i . For that, the V_S has the lower energy of these two defects. Figure 8c shows that in the case of the S-rich limit, the V_S has a negative formation energy if the E_F drops below the 0.68 eV above the E_V . The V_S (S vacancy) will spontaneously form if the E_F moves toward E_V and hinders the p-type doping by opposite charge compensation of V_S . The Fermi energy of 0.68 eV is the "p-type pinning energy" (or p-type limit).⁵² Therefore, in the case of S-rich, the energy range where we can shift E_F by doping without spontaneously forming opposite charge compensating defects is between these two limit energies and yields 1.33 eV.

The analysis is the same if applied to Ca-rich (or S-poor) conditions. Figure 11c shows that both n- and p-type limit energies increase by 2.50 eV which is the half of the calculated formation enthalpy of crystal CaS discussed in the earlier section (the factor divided by the charge of the defect, 2). The energy range for which any native compensating defect does not form spontaneously is still 1.33 eV, from 3.18 to 4.51 eV for E_F , determined by V_S^{2+} and V_{Ca}^{2-} , respectively. Accordingly, the CaS can be dopable in both n-type and p-type but with narrow dopable range for E_F variation, denoting the deep trap levels. The pinning-limit energies for doping in CaS is illustrated in a schematic band diagram as shown in Figure 11d. We set the 0 eV level as the vacuum level for CaS, and the conduction band edge is decided by the calculated electron affinity energy (EA), which is 3.94 eV below the vacuum level. The n-type and p-type limit energy range is shown as an orange shaded area in Figure 11d.

CONCLUSIONS

We have investigated the persistent luminescence mechanism of CaS/Eu²⁺, Dy³⁺ based on our first-principles calculations. Particular attention has been paid to the native point defects and dopants levels in terms of electronic properties and formation energies. We found that the neutral S vacancy has the lowest

energy of 0.62 eV under the Ca-rich limit. The Schottky defect pair defect is another dominant defect with a cost of 1.51 eV per defect site from S-rich to Ca-rich chemical potential limits. Our calculations on the thermodynamic transition levels confirm the experimentally observed intrinsic blue two-peak broad band emissions stimulated by near-infrared range irradiation for undoped CaS. Both Eu and Dy show energetically favorable trends to be substitutionally doped in the CaS lattice. All of the positive charge states of the Eu ion contribute a localized recombination trapping level in the gap, while they have very deep donor transition level. The neutral state of Dy contributes the eoccupied 4f level localized 1.3 eV below the conduction band edge with very shallow donor type transition level (0+) of 0.56 eV below the conduction band. All of the positive charge states of Dy have two shallow 5d levels with 0.4 and 0.6 eV below the conduction band. It is suggested that the Eu ionic doping level controls luminescence wavelength. To prolong the persistent luminescence time, it is preferred to induce the neutral Dy doping site for deep 4f level localized in the band gap. To reduce the activation barrier and increase stronger intensity, the positive Dy ionic doping sites should also be taken into account. We further analyzed that the Dy dopant contributed deeper trap levels in the CaS materials that can store the electron carriers with more evenly, with wider and deeper range of levels being distributed so that prolong the decay-time of the persistent luminescence. The related 980 nm photo-stimulated luminescence is actualized with the help of native defects like V_S^0 , V_S^+ , and STK^- as a relay center for a possible up-converted luminescence. We also summarized a narrow doping limit energy, which has been determined as 1.33 eV constantly in CaS independent of different chemical potential limits. There are advantages to us using the defect level study combined with formation energies to suggest doping energy limits and explain the photostimulated luminescence in terms of native point defects.

AUTHOR INFORMATION

Corresponding Author

*E-mail: bhuang@polyu.edu.hk.

Present Address

Department of Applied Biology and Chemical Technology, The Hong Kong Polytechnic University, Hung Hom, Kowloon, Hong Kong SAR, China.

Notes

The author declares no competing financial interest.

ACKNOWLEDGMENTS

I gratefully acknowledge the support of Nature Science Foundation of China (NSFC) for Youth Scientist (Grant No. NSFC 11504309), and initial start-up grant support from the department general research fund (Dept. GRF) from ABCT in the Hong Kong Polytechnic University.

REFERENCES

- (1) Hölsä, J. *Electrochim. Soc. Interface* **2009**, *18*, 42–45.
- (2) Matsuzawa, T.; Aoki, Y.; Takeuchi, N.; Murayama, Y. *J. Electrochim. Soc.* **1996**, *143*, 2670–2673.
- (3) Pan, Z.; Lu, Y.-Y.; Liu, F. *Nat. Mater.* **2012**, *11*, 58–63.
- (4) Maldiney, T.; Bessière, A.; Seguin, J.; Teston, E.; Sharma, S. K.; Viana, B.; Bos, A. J. J.; Dorenbos, P.; Bessodes, M.; Gourier, D.; Scherman, D.; Richard, C. *Nat. Mater.* **2014**, *13*, 418–426.
- (5) Allix, M.; Chenu, S.; Véron, E.; Poumeyrol, T.; Kouadri-Boudjelthia, E. A.; Alahraché, S.; Porcher, F.; Massiot, D.; Fayon, F. *Chem. Mater.* **2013**, *25*, 1600–1606.
- (6) Lecointre, A.; Bessière, A.; Bos, A. J. J.; Dorenbos, P.; Viana, B.; Jacquot, S. *J. Phys. Chem. C* **2011**, *115*, 4217–4227.
- (7) Rodríguez Burbano, D. C.; Sharma, S. K.; Dorenbos, P.; Viana, B.; Capobianco, J. A. *Adv. Opt. Mater.* **2015**, *3*, 551–557.
- (8) Liu, F.; Liang, Y.; Pan, Z. *Phys. Rev. Lett.* **2014**, *113*, 177401.
- (9) Liu, X.; Yan, C.-H.; Capobianco, J. A. *Chem. Soc. Rev.* **2015**, *44*, 1299–1301.
- (10) Van den Eeckhout, K.; Poelman, D.; Smet, P. *Materials* **2013**, *6*, 2789–2818.
- (11) Dorenbos, P. *J. Electrochim. Soc.* **2005**, *152*, H107–H110.
- (12) Smet, P. F.; Moreels, I.; Hens, Z.; Poelman, D. *Materials* **2010**, *3*, 2834–2883.
- (13) Rinke, P.; Schleife, A.; Kioupakis, E.; Janotti, A.; Rödl, C.; Bechstedt, F.; Scheffler, M.; Van de Walle, C. G. *Phys. Rev. Lett.* **2012**, *108*, 126404.
- (14) Huang, K.; Rhys, A. *Proc. R. Soc. London, Ser. A* **1950**, *204*, 406–423.
- (15) Qu, B.; Zhang, B.; Wang, L.; Zhou, R.; Zeng, X. C. *Chem. Mater.* **2015**, *27*, 2195–2202.
- (16) Rodriguez Burbano, D. C.; Rodriguez, E. M.; Dorenbos, P.; Bettinelli, M.; Capobianco, J. A. *J. Mater. Chem. C* **2014**, *2*, 228–231.
- (17) Qiu, J.; Miura, K.; Inouye, H.; Fujiwara, S.; Mitsuyu, T.; Hirao, K. *J. Non-Cryst. Solids* **1999**, *244*, 185–188.
- (18) Qiu, J.; Kawasaki, M.; Tanaka, K.; Shimizugawa, Y.; Hirao, K. *J. Phys. Chem. Solids* **1998**, *59*, 1521–1525.
- (19) Qiu, J.; Hirao, K. *Solid State Commun.* **1998**, *106*, 795–798.
- (20) Clark, S. J.; Robertson, J.; Lany, S.; Zunger, A. *Phys. Rev. B: Condens. Matter Mater. Phys.* **2010**, *81*, 115311.
- (21) Pacchioni, G.; Frigoli, F.; Ricci, D.; Weil, J. A. *Phys. Rev. B: Condens. Matter Mater. Phys.* **2000**, *63*, 054102.
- (22) Lany, S.; Zunger, A. *Phys. Rev. B: Condens. Matter Mater. Phys.* **2009**, *80*, 085202.
- (23) Anisimov, V. I.; Aryasetiawan, F.; Lichtenstein, A. I. *J. Phys.: Condens. Matter* **1997**, *9*, 767.
- (24) Clark, S. J.; Segall, M. D.; Pickard, C. J.; Hasnip, P. J.; Probert, M. I. J.; Refson, K.; Payne, M. C. Z. *Kristallogr. - Cryst. Mater.* **2005**, *220*, 567–570.
- (25) Kleinman, L.; Bylander, D. M. *Phys. Rev. Lett.* **1982**, *48*, 1425–1428.
- (26) Louie, S. G.; Froyen, S.; Cohen, M. L. *Phys. Rev. B: Condens. Matter Mater. Phys.* **1982**, *26*, 1738–1742.
- (27) Rappe, A. M.; Rabe, K. M.; Kaxiras, E.; Joannopoulos, J. D. *Phys. Rev. B: Condens. Matter Mater. Phys.* **1990**, *41*, 1227–1230.
- (28) Hasnip, P. J.; Pickard, C. J. *Comput. Phys. Commun.* **2006**, *174*, 24–29.
- (29) Laasonen, K.; Pasquarello, A.; Car, R.; Lee, C.; Vanderbilt, D. *Phys. Rev. B: Condens. Matter Mater. Phys.* **1993**, *47*, 10142–10153.
- (30) Marzari, N.; Vanderbilt, D.; Payne, M. C. *Phys. Rev. Lett.* **1997**, *79*, 1337–1340.
- (31) Lany, S.; Zunger, A. *Phys. Rev. B: Condens. Matter Mater. Phys.* **2010**, *81*, 205209.
- (32) Morgan, B. J.; Watson, G. W. *J. Phys. Chem. C* **2010**, *114*, 2321–2328.
- (33) Keating, P. R. L.; Scanlon, D. O.; Morgan, B. J.; Galea, N. M.; Watson, G. W. *J. Phys. Chem. C* **2011**, *116*, 2443–2452.
- (34) Huang, B.; Gillen, R.; Robertson, J. *J. Phys. Chem. C* **2014**, *118*, 24248–24256.
- (35) Probert, M. I. J.; Payne, M. C. *Phys. Rev. B: Condens. Matter Mater. Phys.* **2003**, *67*, 075204.
- (36) Denlinger, J. D.; Clack, J. A.; Allen, J. W.; Gweon, G. H.; Poirier, D. M.; Olson, C. G.; Sarrao, J. L.; Bianchi, A. D.; Fisk, Z. *Phys. Rev. Lett.* **2002**, *89*, 157601.
- (37) Tromp, H. J.; van Gelderen, P.; Kelly, P. J.; Brocks, G.; Bobbert, P. A. *Phys. Rev. Lett.* **2001**, *87*, 016401.
- (38) Wu, Z.; Singh, D. J.; Cohen, R. E. *Phys. Rev. B: Condens. Matter Mater. Phys.* **2004**, *69*, 193105.
- (39) Gao, S.-P.; Jiang, J.; Cao, M.; Zhu, J.; Yuan, J. *Phys. Rev. B: Condens. Matter Mater. Phys.* **2004**, *69*, 214419.

- (40) Clark, S. J.; Robertson, J. *Phys. Rev. B: Condens. Matter Mater. Phys.* **2010**, *82*, 085208.
- (41) Huang, B. *J. Comput. Chem.*, accepted (2015).
- (42) Lany, S.; Zunger, A. *Phys. Rev. B: Condens. Matter Mater. Phys.* **2008**, *78*, 235104. Lany, S.; Zunger, A. *Phys. Rev. B: Condens. Matter Mater. Phys.* **2005**, *72*, 035215.
- (43) Poncé, S.; Bertrand, B.; Smet, P. F.; Poelman, D.; Mikami, M.; Gonze, X. *Opt. Mater.* **2013**, *35*, 1477–1480.
- (44) Waroquier, D.; Lherbier, A.; Miglio, A.; Stankovski, M.; Poncé, S.; Oliveira, M. J. T.; Giantomassi, M.; Rignanese, G.-M.; Gonze, X. *Phys. Rev. B: Condens. Matter Mater. Phys.* **2013**, *87*, 075121.
- (45) Lide, D. R.; Kahiaian, H. V. *CRC Handbook of Thermophysical and Thermochemical Data*; CRC Press: Boca Raton, FL, 1994.
- (46) Karsai, F.; Tiwald, P.; Laskowski, R.; Tran, F.; Koller, D.; Gräfe, S.; Burgdörfer, J.; Wirtz, L.; Blaha, P. *Phys. Rev. B: Condens. Matter Mater. Phys.* **2014**, *89*, 125429.
- (47) Pandey, R.; Kunz, A. B.; Vail, J. M. *J. Mater. Res.* **1988**, *3*, 1362–1366.
- (48) Pandey, R.; Harding, J. H. *Philos. Mag. B* **1984**, *49*, 135–141.
- (49) Pandey, R.; Stoneham, A. M. *J. Phys. C: Solid State Phys.* **1985**, *18*, 5289.
- (50) Dorenbos, P. *Phys. Rev. B: Condens. Matter Mater. Phys.* **2012**, *85*, 165107.
- (51) Dorenbos, P. *J. Lumin.* **2013**, *135*, 93–104.
- (52) Robertson, J.; Clark, S. J. *Phys. Rev. B: Condens. Matter Mater. Phys.* **2011**, *83*, 075205.
- (53) Zhang, S. B.; Wei, S.-H.; Zunger, A. *J. Appl. Phys.* **1998**, *83*, 3192–3196.